CHAPTER IV
RESULTS AND DISCUSSION

4.1 Au/CeO_2 Catalysts

In this part, Au/CeO_2 catalysts were prepared by deposition-precipitation (DP) and characterized by several techniques. The prepared catalysts were tested in the oxidative methanol reforming reaction. Moreover, the effects of H_2O/CH_3OH molar ratio, O_2/CH_3OH molar ratio, Au content, calcination temperature, and reaction temperature on the catalytic performance were studied in detail.

The catalytic activity tests were carried out in a vertical pyrex glass microreactor by packing with 100 mg catalyst of 80–120 mesh inside. The activity was investigated at varied temperature in the range of 200 to 400°C under atmospheric pressure. The characterization results from several techniques including TPR, FT-IR, UV-vis, XRD, TEM, TPO, AAS, and BET surface area of the prepared catalysts were used to explain the catalytic activity and selectivity of the prepared catalysts in this part.

4.1.1 Effect of H_2O/CH_3OH Molar Ratio on the Catalytic Performance of 1% Au/CeO_2

To study the effect of H_2O/CH_3OH molar ratio on the catalytic performance of 1%wt Au/CeO_2, the catalysts were tested with various H_2O/CH_3OH molar ratios at 1/1, 2/1, 3/1, and 4/1, respectively, with reaction temperature. The catalysts were prepared by deposition-precipitation technique with 1%wt of Au content and calcined at 400°C for 4 hours. Figure 4.1 shows the methanol conversion and hydrogen yield in the OSRM reaction with different H_2O/CH_3OH molar ratios during the reaction temperature from 200 to 400°C.

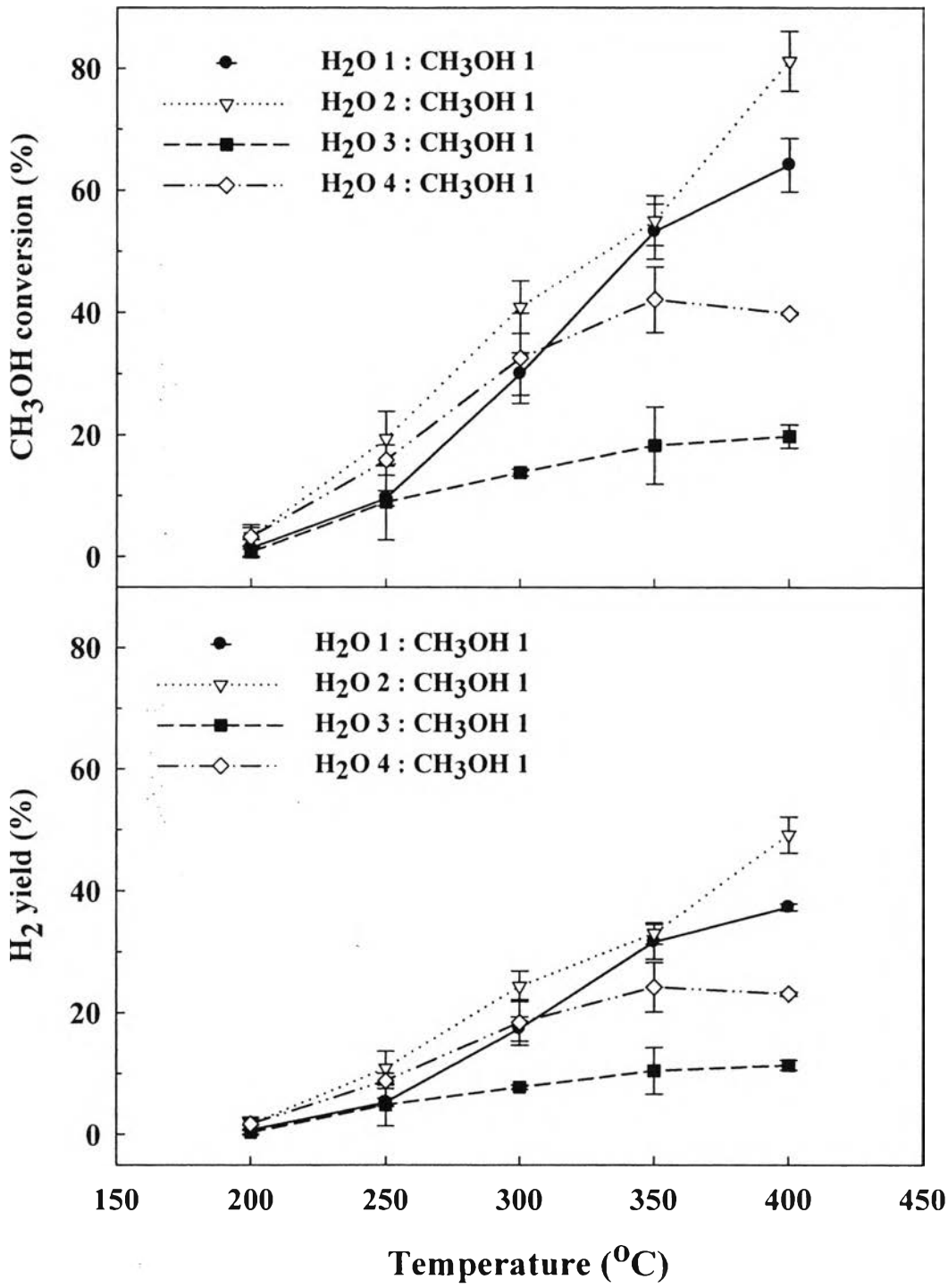

Figure 4.1 Effect of H_2O/CH_3OH molar ratio on the methanol conversion and hydrogen yield over 1%wt Au/CeO_2 catalysts calcined at 400°C.

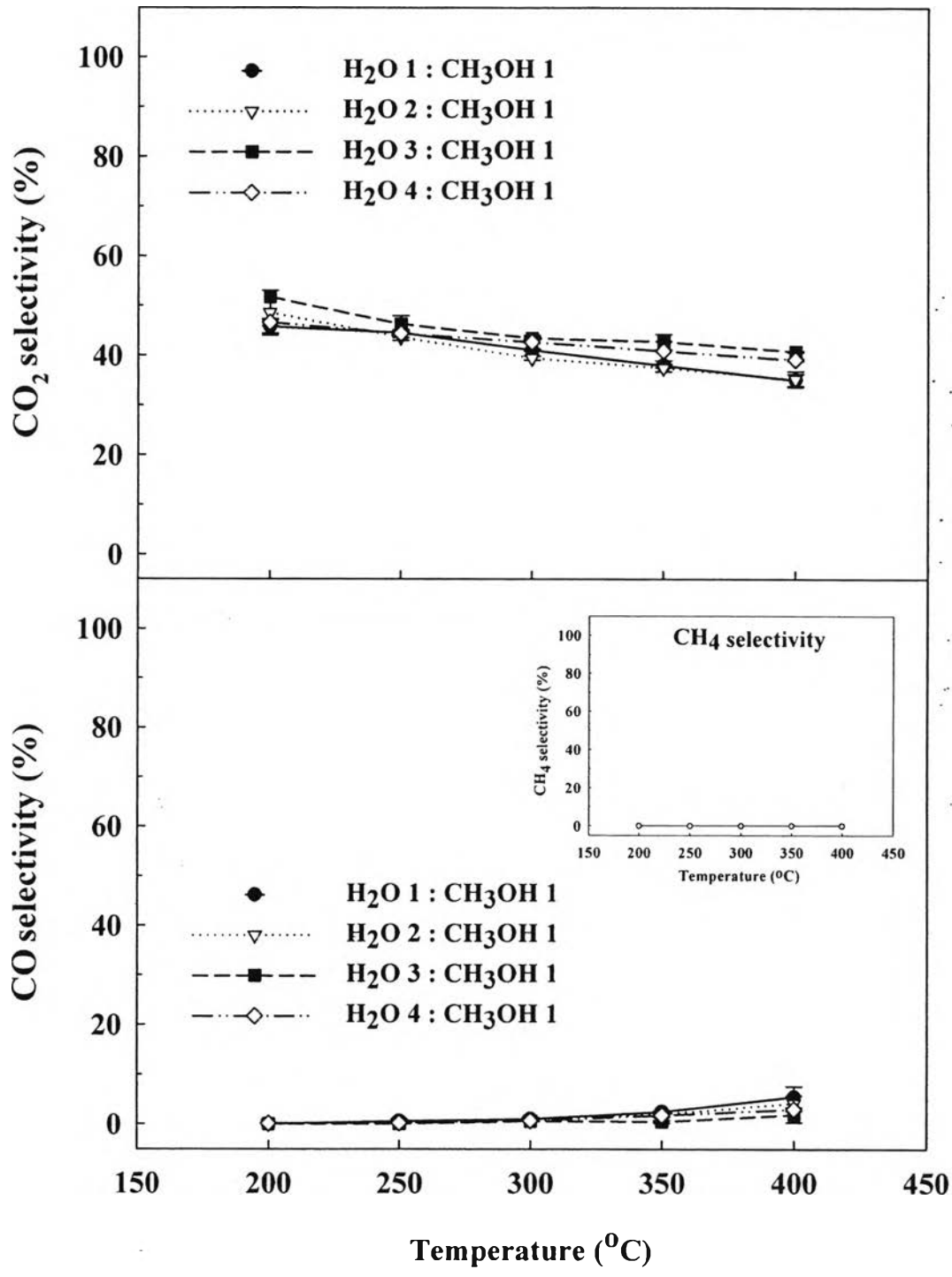

Figure 4.2 Effect of H_2O/CH_3OH molar ratio on CO_2, CO, and CH_4 selectivity over 1%wt Au/CeO_2 catalysts calcined at 400°C.

It can be seen that the methanol conversion and hydrogen yield increased with reaction temperature at all H_2O/CH_3OH molar ratios since the addition of steam led to the SRM, which corresponded to the endothermic reaction. In addition, it is strongly affected by the H_2O/CH_3OH ratio. For the appropriate ratio, the H_2O/CH_3OH molar ratio at 2/1 exhibited the highest catalytic activity with the highest methanol conversion and hydrogen yield in the whole range of reaction temperature (200 to 400°C) compared to other H_2O/CH_3OH molar ratios. After increasing the H_2O/CH_3OH molar ratios up to 3/1, the catalytic activity decreased significantly. This can be explained by the formation of hydroxyl groups and carbonate species which blocked the active sites of catalysts during the reaction. Generally, there are many side reactions occurring including steam reforming reaction with high amount of steam content in the feedstream. This corresponded to the accumulation of many types of carbonate species—adsorbed reaction intermediates—on the active sites (Tabakova *et al.,* 2003). When increasing the H_2O/CH_3OH molar ratio up to 4/1, the catalytic activity turned to increase dramatically, but still lower than the H_2O/CH_3OH molar ratio at 2/1 for both methanol conversion and hydrogen yield. It has been reported that the appropriate steam can decompose the carbonate species, which blocked the active sites (El-Moemen *et al.,* 2008). Then, the catalysts turn to reactivate again (El-Moemen *et al.,* 2008). However, in this work the hydroxyl groups and carbonate species were detected by FT-IR technique. In Figure 4.2, all H_2O/CH_3OH molar ratios showed a CO selectivity of slightly less than 10% for all temperature range. However, no methane product was observed in this reaction. The higher reaction temperature, the higher CO content since the methanol decomposition could act as the main side reaction. Consequently, the H_2O/CH_3OH molar ratio of 2/1 was chosen as the optimum condition for further studying and improving the catalytic performance at low temperature range of 200–300°C in the next parameter. In the region where the low temperature range covered at this optimum ratio, the highest methanol conversion and hydrogen yield exceeded 41% and 24%, respectively.

4.1.1.1 Fourier Transform Spectroscopy (FT-IR)

The FT-IR results of the spent 1%Au/CeO_2 catalysts with different H_2O/CH_3OH molar ratios are shown in Figure 4.3 (a) and (b) for both hydroxyl groups and carbonate species, respectively. For hydroxyl groups, a board transmission in OH region was observed in negative band in the range of 3200–3600 cm^{-1}, which followed to the OH stretching mode of water molecules (El-Moemen *et al.*, 2008). Compared to fresh 1%Au/CeO_2 catalyst, the band of OH group was presented with the strong signal of transmittance for all spent catalysts. The slight difference in frequency detected for the bands of OH groups in comparison with each spent catalyst may be due to different H_2O/CH_3OH molar ratios. On the other hand, the carbonate species on the surface were obviously detected in many positions including unspecified carbonate species in the range of 800–1800 cm^{-1} and 2500–3000 cm^{-1}. Many literature reviews proposed that the formation of adsorbed carbonate or formate species with many different possible pathways. Costello *et al.* (2003) suggested that the first possible pathway of the carbonate formation at the active site of Au/Al_2O_3 catalysts was the dehydration of the surface bicarbonate intermediate (-CO_3H) and an adjacent hydroxyl (OH^-), as shown in Eq. 4.1.

$$Au\text{–}(CO_3H) + Al\text{–}OH \longrightarrow Au\text{–}(CO_3)\text{–}Al + H_2O \qquad (4.1)$$

As described previously, they also reported another pathway for the carbonate formation while using Au as the metal with different supports. Eq. (4.2) shows the formation of carbonate by reacting the bicarbonate with another Au–OH.

$$Au\text{–}(CO_3H) + Au\text{–}OH \longrightarrow Au\text{–}(CO_3)\text{–}Au + H_2O \qquad (4.2)$$

All of these species were identified as the main cause of catalyst deactivation resulting from the blocking in active sites by intermediate formation or blocking the access of adsorbed reaction intermediates to the active sites (El-Moemen *et al.*, 2008). The different intensity of each peak indicated the different kinds of carbonate species including formate species, as shown in Table 4.1. Interestingly, the spent catalyst carried out at the H_2O/CH_3OH of 3/1 showed the appearance of the strong

bands at 2853, and at 2924 and 2955 cm^{-1}, relating to the formate species on Ce^{3+} and Ce^{4+}, respectively. These formate intermediate species could also definitely block the active sites. Moreover, it can be explained that the high amount of water led to the WGS reaction which was the side reaction during the SRM reaction and also related to the formate species as the intermediates during the reaction (El-Moemen *et al.*, 2008). This phenomenon strongly reduced the catalytic performance of 1%wt. Au/CeO_2 catalyst at H_2O/CH_3OH molar ratio of 3/1 which corresponded to the lowest methanol conversion and hydrogen yield. However, the formate species decreased significantly after increasing the H_2O/CH_3OH to 4/1 since the appropriate amount of steam might lead to the decomposition of the formate species on the active sites, as shown in Figure 4.3 (a) (Tabakova *et al.*, 2003). Consequently, the catalytic activity turned to activate again, but was still less than the H_2O/CH_3OH ratio of 2/1. For the Figure 4.3 (b), the carbonate species could also be observed in another wavenumbers. These carbonate species could also block the active sites similar to formate species (El-Moemen *et al.*, 2008). Nevertheless, the intensity of the peaks of carbonate species became weaker at higher H_2O/CH_3OH ratio than 2/1 since the high amount of water can easily reduce the carbonate species with decomposition of carbonate species when the catalyst was heated with high steam content during the reaction (El-Moemen *et al.*, 2008). Finally, the intensities of all the bands related to different kind of carbonate species decreased. A potential for mechanism for the decomposition of carbonates—known as the reverse carbonate formation—via the less stable bicarbonate has been proposed by Costello *et al.* (2003) and Calla *et al.* (2006), as represented by Eqs. 4.2–4.3.

$$CO_3^{2-} + H_2O \longrightarrow CO_3H^- + OH^- \quad (4.3)$$

$$CO_3H^- \longrightarrow CO_2 + OH^- \quad (4.4)$$

Interestingly, the carbonate species became lowest with the lowest catalytic activity at the H_2O/CH_3OH molar ratio of 3/1. This could be implied that the catalytic performance might depend on the formate species stronger than the carbonate species. After increasing the H_2O/CH_3OH molar ratio to 4/1, the carbonate species turned to increase with the decrease in formate species. This was in line with Jacobs

et al. (2004) that the high amount of steam could further convert the formate species to unidentate carbonate being the precursor leading to CO_2 as the final product. However, it was speculated that the formate species might be the main cause for getting the lower catalytic activity. In conclusion, this was reasonable to follow that the catalytic performance at the optimum condition depends on the amount of remaining carbonate and formate species on the active sites.

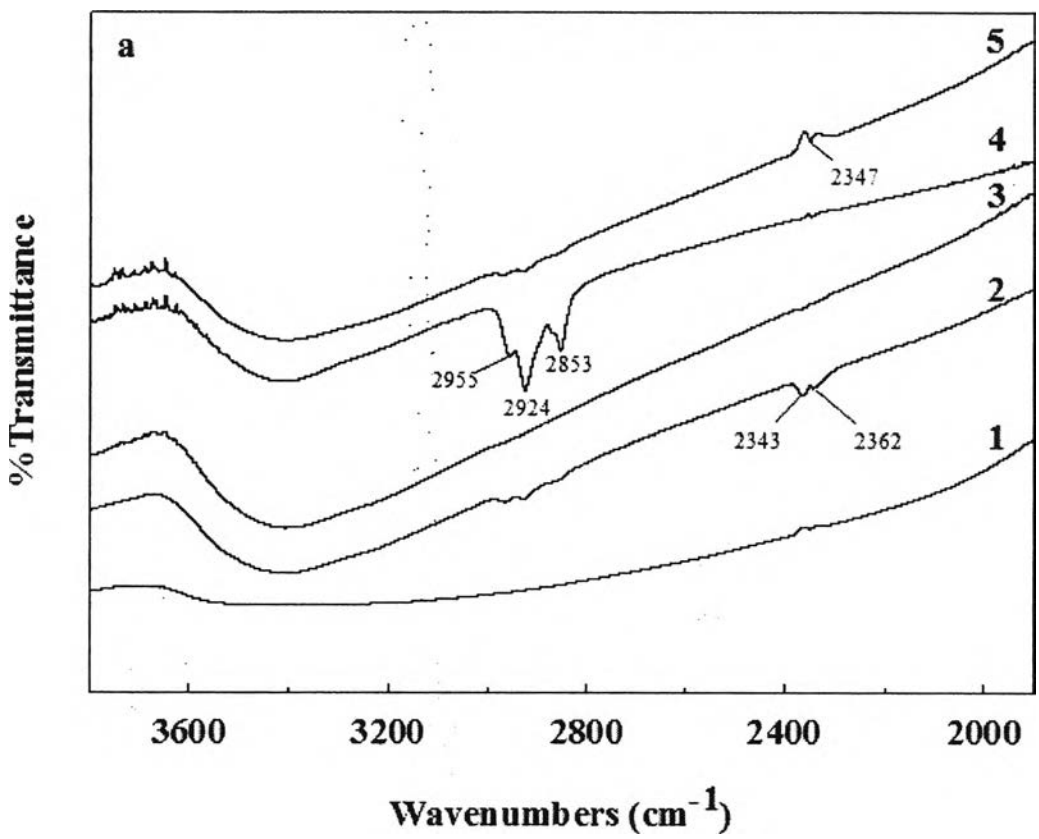

Figure 4.3 FTIR spectra of 1%wt Au/CeO_2 catalysts calcined at 400°C. (a) (1) Fresh catalyst; (2) after reaction at H_2O/CH_3OH molar ratio of 1/1; (3) after reaction at H_2O/CH_3OH molar ratio of 2/1; (4) after reaction at H_2O/CH_3OH molar ratio of 3/1; (5) after reaction at H_2O/CH_3OH molar ratio of 4/1.

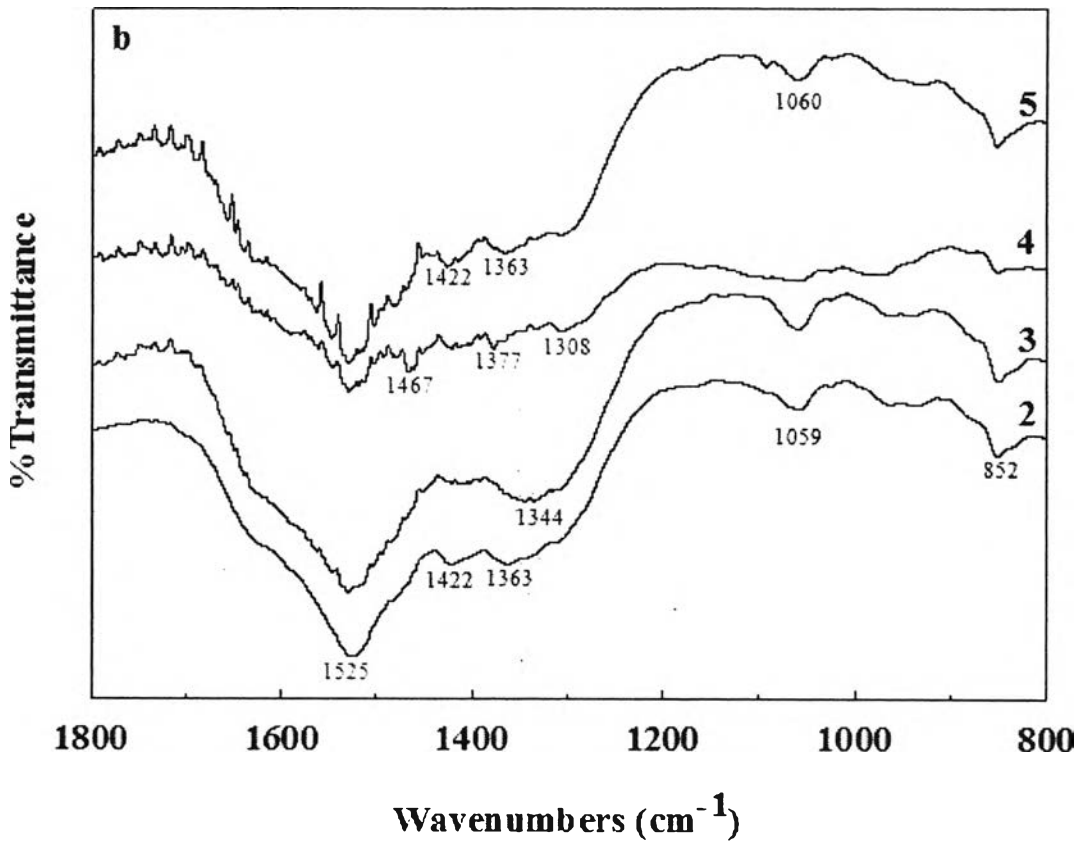

Figure 4.3 FTIR spectra in the carbonate region recorded after SRM reaction performed on 1%wt Au/CeO_2 catalysts calcined at 400°C. (b) (2) After reaction at H_2O/CH_3OH molar ratio of 1/1; (3) after reaction at H_2O/CH_3OH molar ratio of 2/1; (4) after reaction at H_2O/CH_3OH molar ratio of 3/1; (5) after reaction at H_2O/CH_3OH molar ratio of 4/1.

Table 4.1 Frequency and assignment of carbonate, formate, and intermediate bands on spent 1%wt Au/CeO_2 calcined at 400°C (Tabakova *et al.*, 2003)

Wavenumber (ν, cm^{-1})	Assignment
2853, 1585, 1377, 1363	Formate species on Ce^{3+}
2955, 2924, 2963, 2928, 1377, 1363	Formate species on Ce^{4+}
1308, 1632	Formate species on Au
1467, 1422, 1344, 1070–1045, 852	Carbonate species on Ceria
1525	Bicarbonate species on Ceria
2347, 2343, 2368	Linear CO_2 weakly interacting with ceria

4.1.2 Effect of O_2/CH_3OH Molar Ratio on the Catalytic Performance of 1% Au/CeO_2

To evaluate the condition for the oxidative steam reforming reaction over 1%wt Au/CeO_2, the O_2/CH_3OH molar ratios were varied from 0 to 0.63, 1.25, 1.88, and 2.50, as shown on Figures 4.4–4.6, while keeping the optimum condition of the H_2O/CH_3OH molar ratio at 2/1 constant. Figure 4.4 shows the methanol conversion and hydrogen yield in the OSRM reaction with different O_2/CH_3OH molar ratios at reaction temperature of 200 to 400°C. The methanol conversion enhanced extremely in the whole range of reaction temperature with the addition of oxygen into the reaction according to the combination and competition between SRM and POM reactions. It can be seen that at a feed O_2/CH_3OH molar ratio 1.25/1, the methanol conversion was higher than 90% at 250°C and continuously rised up to 98.63% at 400°C. Nevertheless, the hydrogen yield decreased at temperature higher than 300°C. Significantly improving of hydrogen yield was observed with this ratio in the low temperature range around 200–300°C compared to other ratios. It indicated that the appropriate concentration of the mixture among oxygen, steam, and methanol in the feedstream resulted in the combination of SRM and POM which led to the high activity at low temperatures for hydrogen production during the oxidative steam reforming of methanol (OSRM). In contrast, too much oxygen (O_2/CH_3OH) can give a fast catalyst deactivation and hydrogen consumption via hydrogen

oxidation. Some researchers also achieved the same results that the hydrogen production rate significantly decreased with increasing the O_2/CH_3OH molar ratio because of POM reaction while the methanol conversion was still 100% (Patel *et al.*, 2007). The results in Figure 4.5 showed that the addition of oxygen decreased the hydrogen selectivity than the absence of oxygen which preferred to SRM. Compared to SRM: to identify either the similarities or the differences between two things, OSRM has a higher reaction rate, which results in a higher hydrogen production and a higher hydrogen partial pressure in the side reaction. The more oxygen contents were added into the reaction, the more reactions preferred to POM which is not favorable at high temperature due to its exothermic reaction. With the highest O_2/CH_3OH molar ratio of 2.50, the POM reaction caused the most effective way to the lowest hydrogen selectivity compared to SRM which was also in accordance with the highest selectivity. In this way, the appropriate O_2/CH_3OH molar ratio of 1.25 represented the higher selectivity in the low temperature range around 200–300°C, but still lower than SRM. This evidence can insist definitely the appearance of the OSRM during the optimum condition. It has been reported that OSRM reduced CO levels with the H_2 selectivity: SRM>OSRM>POM (Agrell *et al.*, 2003). Surprisingly, the CO selectivity increased when increasing the O_2/CH_3OH molar ratio to 1.25, and then decreased with higher O_2/CH_3OH molar ratio, as shown in Figure 4.6. At an O_2/CH_3OH molar ratio of 1.25, the methanol decomposition might contribute the CO formation in large extent. After that, when feeding more oxygen than this ratio might suppress the CO formation by passing through two possible pathways—CO oxidation and water gas shift reaction—which were selective to the roles of Au/CeO_2 catalyst in the whole temperature range (El-Moemen *et al.*, 2008) and there was no methane detected during the reaction. In conclusion, $O_2/H_2O/CH_3OH$ molar ratio at 1.25/2/1 exhibited the highest catalytic activity in OSRM with the highest methanol conversion and hydrogen yield in the range of low temperature from 200 to 300°C compared to other molar ratios.

The methanol conversion and hydrogen yield increased with increasing O_2/CH_3OH molar ratio up to 1.25. At this ratio, methanol conversion reached to a maximum value and beyond that the hydrogen yield declined with further increase in the O_2/CH_3OH molar ratio to 2.5. Nevertheless, hydrogen yield

decreased dramatically to almost zero compared to initial molar ratio since the influence of partial oxidation, which produces 2 moles of hydrogen per one mole of methanol. In fact, the POM is more pronounced in the high O_2/CH_3OH molar ratio. This could be explained that the existence of partial oxidation reaction depended on the highest oxygen content in the feed ratio during the OSRM reaction (Patel *et al.*, 2007). To better understand the existence of POM, from the above description, it is not necessary to make the experimental test with 100% purity of O_2 without carrier gas (He). Indeed, the O_2/CH_3OH molar ratio at 2.50/1 was sufficient for studying the POM reaction.

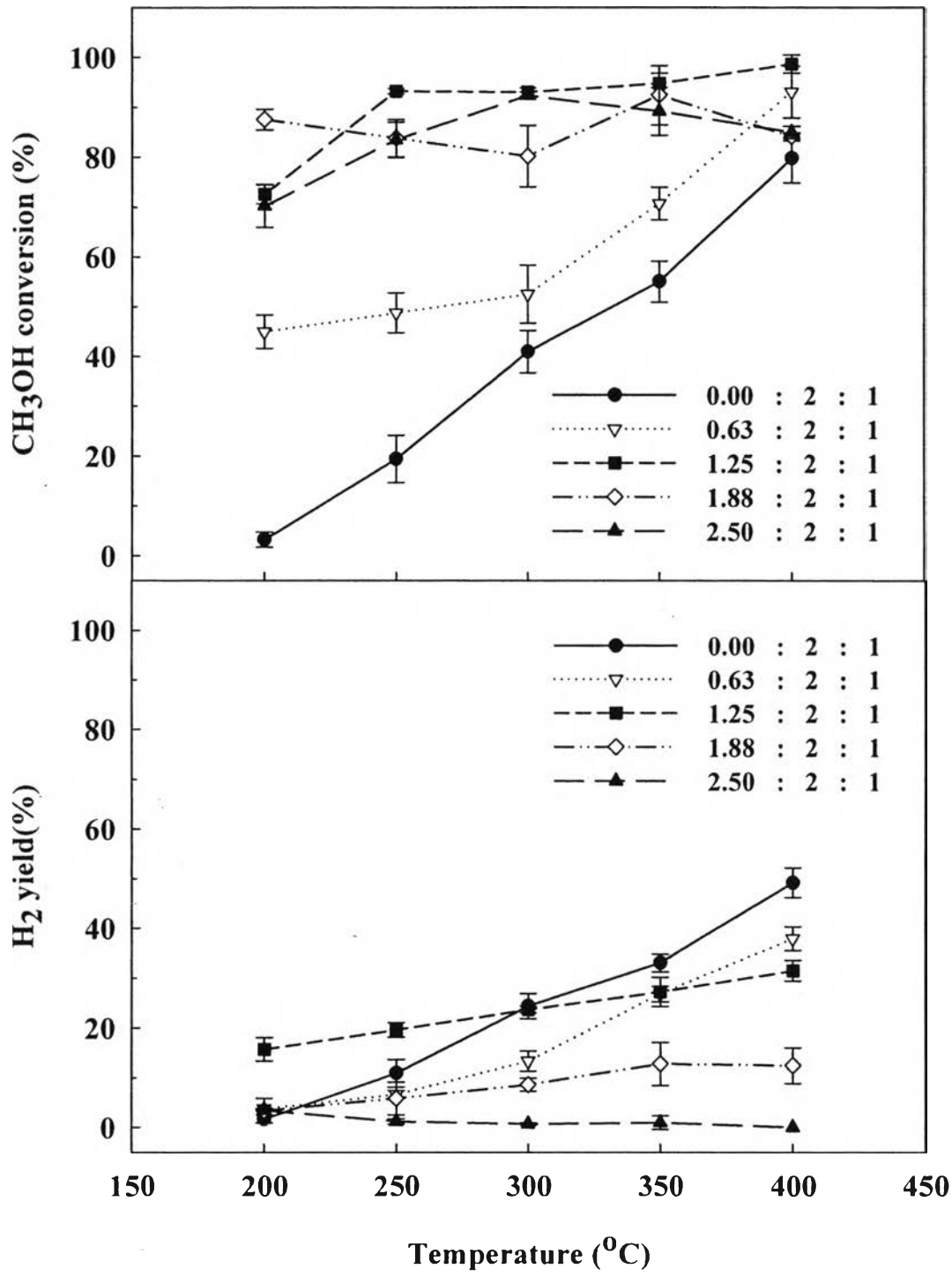

Figure 4.4 Effect of $O_2/H_2O/CH_3OH$ molar ratio on the methanol conversion and hydrogen yield over 1%wt Au/CeO_2 catalysts calcined at 400°C.

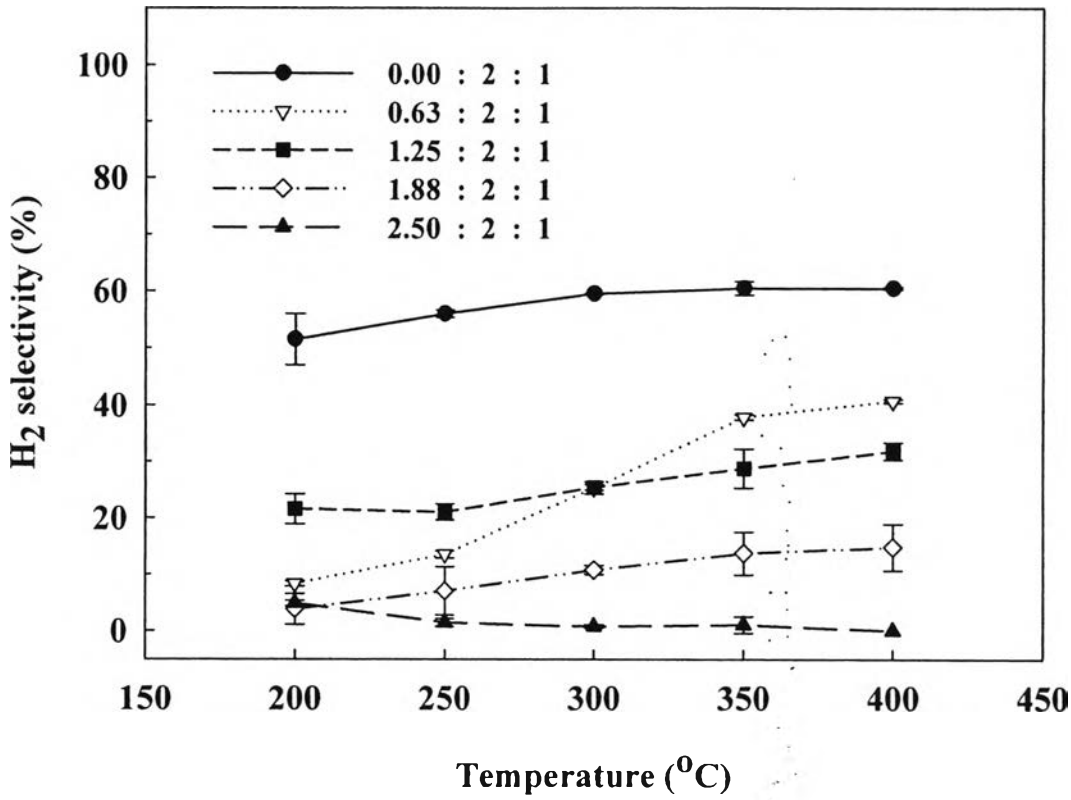

Figure 4.5 Effect of $O_2/H_2O/CH_3OH$ molar ratio on the hydrogen selectivity over 1%wt Au/CeO_2 catalysts calcined at 400°C.

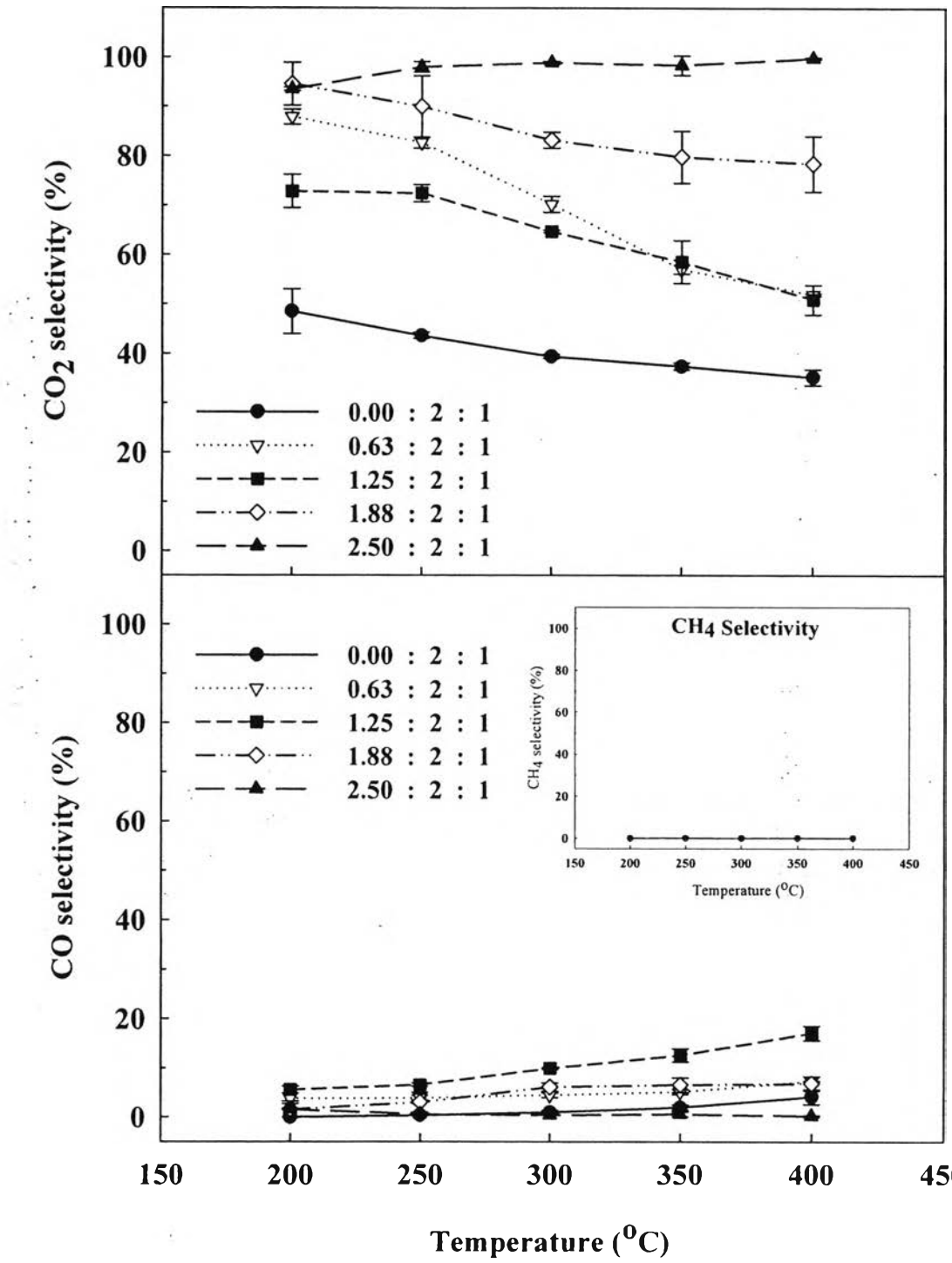

Figure 4.6 Effect of $O_2/H_2O/CH_3OH$ molar ratio on CO_2, CO, and CH_4 selectivity over 1%wt Au/CeO_2 catalysts calcined at 400°C.

4.1.3 Effect of Au Content over CeO_2 Support on the Catalytic Performance

The Au/CeO_2 catalysts were prepared by deposition-precipitation technique with various Au contents of 1%, 3% and 5%wt. All of these catalysts were calcined at 400°C for 4 hours.

The effect of Au content on Au/CeO_2 catalysts on both methanol conversion and hydrogen yield is illustrated in Figure 4.7. It was found that with increasing Au content, methanol conversion was decreased in the range of 200–300°C. At low Au loading (1% Au), Au could be well dispersed and the Au crystallite size becomes small, so the catalytic activity of 1% Au/CeO_2 was high. At 3% Au loading, contrary effects are observed at low temperature range and the 5% Au content exhibited the highest performance (100% methanol conversion), compared to 1% and 3% Au, respectively. It can be seen that there were the slight difference in hydrogen yields in this low temperature range. The hydrogen selectivity also followed as the same trends as the hydrogen yield supporting that there is no extreme improvement when increasing Au loading. It can be concluded that high Au content promoted the CO suppression during the reaction with CO oxidation and WGSR. This corresponded to the increasing of CO_2 selectivity without methane formation, as shown in Figure 4.8.

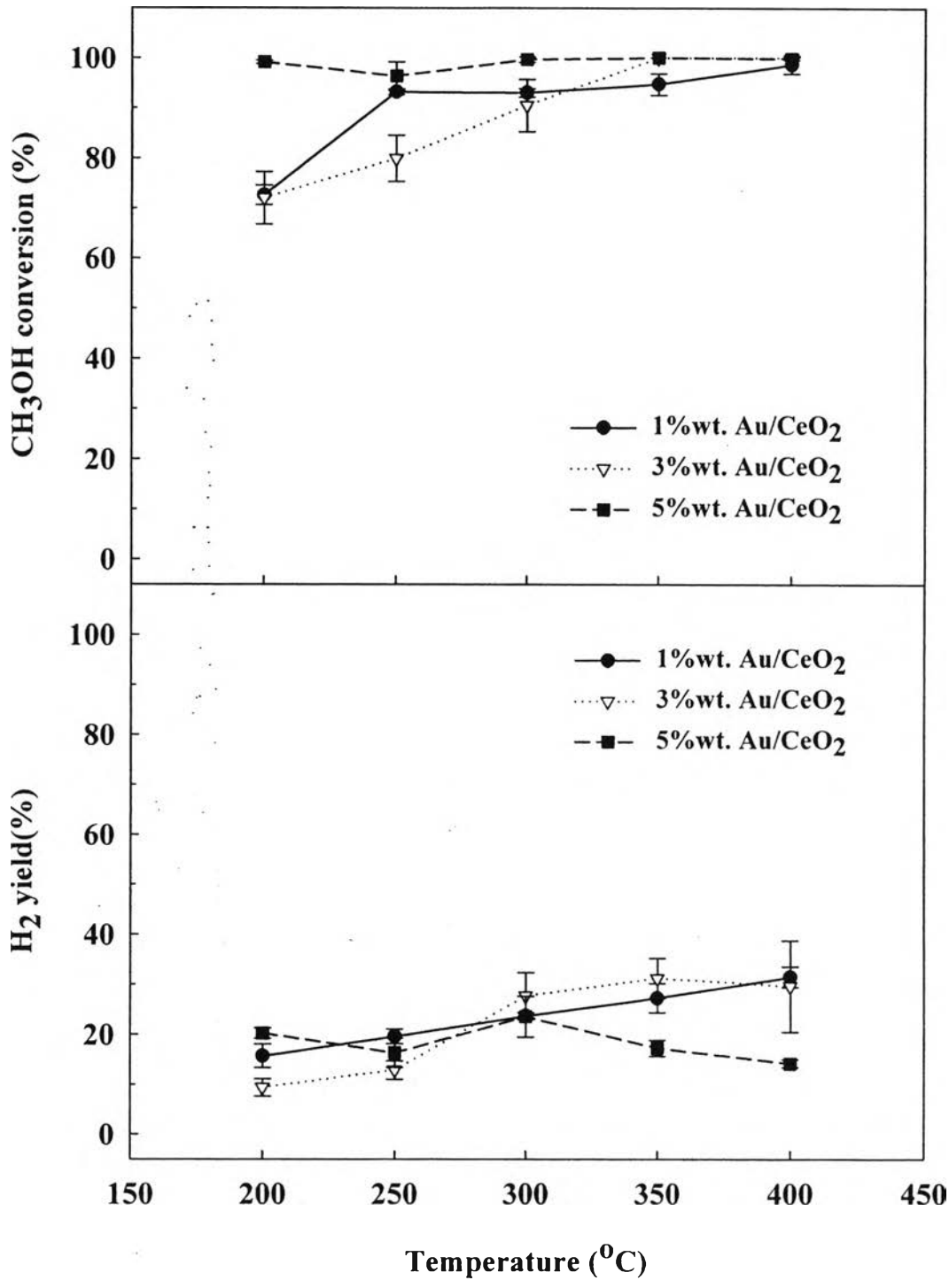

Figure 4.7 Effect of Au loading on methanol conversion and hydrogen yield over Au/CeO_2. Reaction conditions: $O_2/H_2O/CH_3OH$ = 1.25/2/1 and calcination temperature of 400°C.

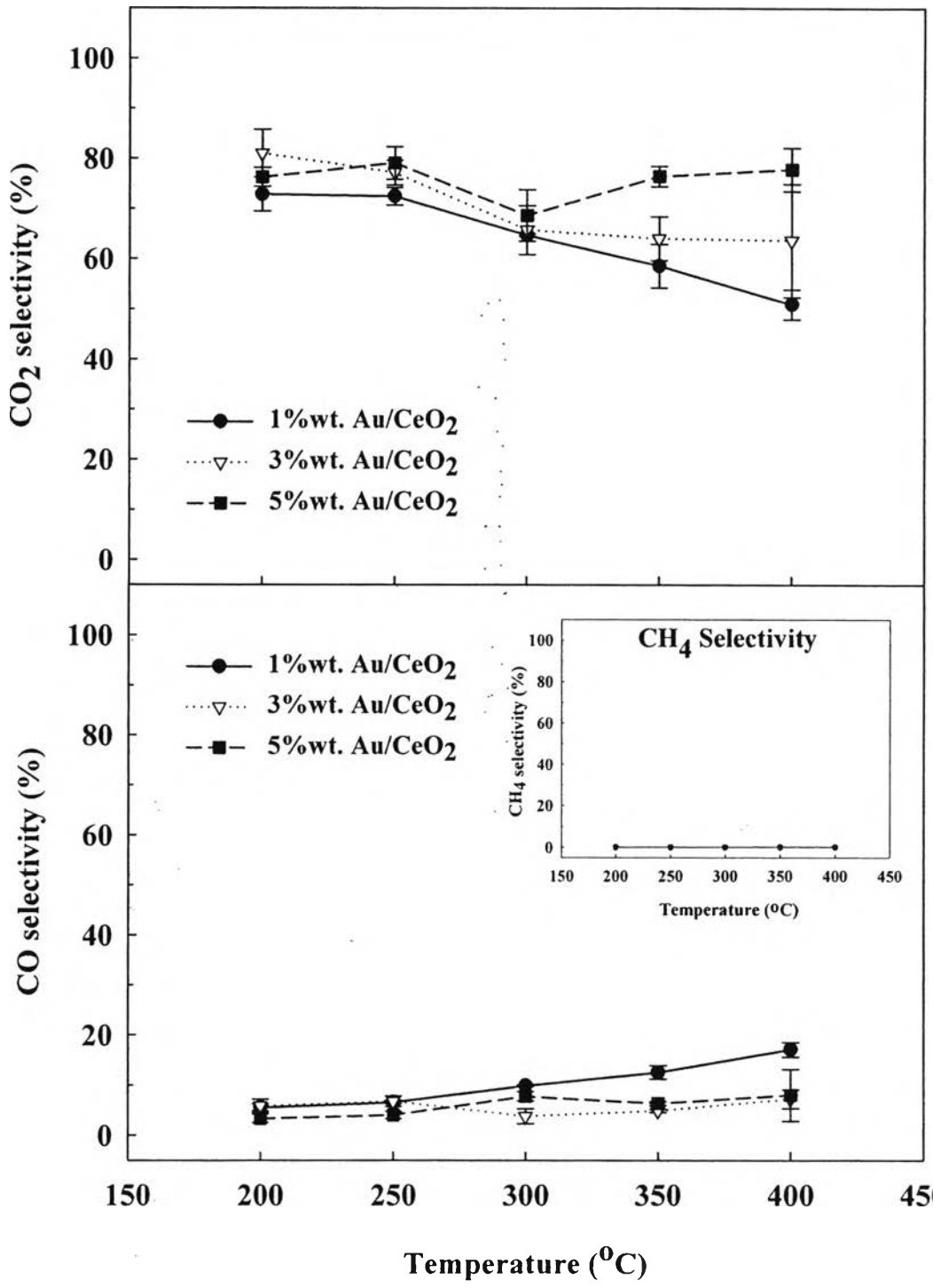

Figure 4.8 Effect of Au loading on CO_2, CO, and CH_4 selectivity over Au/CeO_2. Reaction conditions: $O_2/H_2O/CH_3OH$ = 1.25/2/1 and calcination temperature of 400°C.

4.1.3.1 Atomic Absorption Spectroscopy (AAS)

In order to measure the actual metal loading of Au/CeO_2 catalysts calcined at 400°C, AAS was used and the results of various Au loadings are summarized in Table 4.2.

Table 4.2 Actual metal loading of Au/CeO_2 catalysts

Catalysts	Actual metal loading (%wt.)
1%wt Au/CeO_2	0.86
3%wt Au/CeO_2	2.54
5%wt Au/CeO_2	4.42

4.1.3.2 X-ray Diffraction (XRD)

From Figure 4.9, it is clearly seen that the peak intensity of Au(111) at 38.5° become detectable when the Au loading is at 5%. Apparently, the diffraction of CeO_2 presented a very strong peak at XRD $2\theta = 28.5°$, which was the characteristic of fluorite structure. Similar to previous works, the other detected weak peaks at 33.08, 47.47, 56.33, 59.08, 69.40, 76.69, and 79.07° were corresponding to (200), (220), (311), (222), (400), (331), and (420) for CuKα (1.5406 Å) radiation, respectively (Kunming *et al.*, 2008). The CeO_2 crystalline sizes of Au/CeO_2 catalysts were calculated based on the Scherrer equation and the results are summarized in Table 4.3.

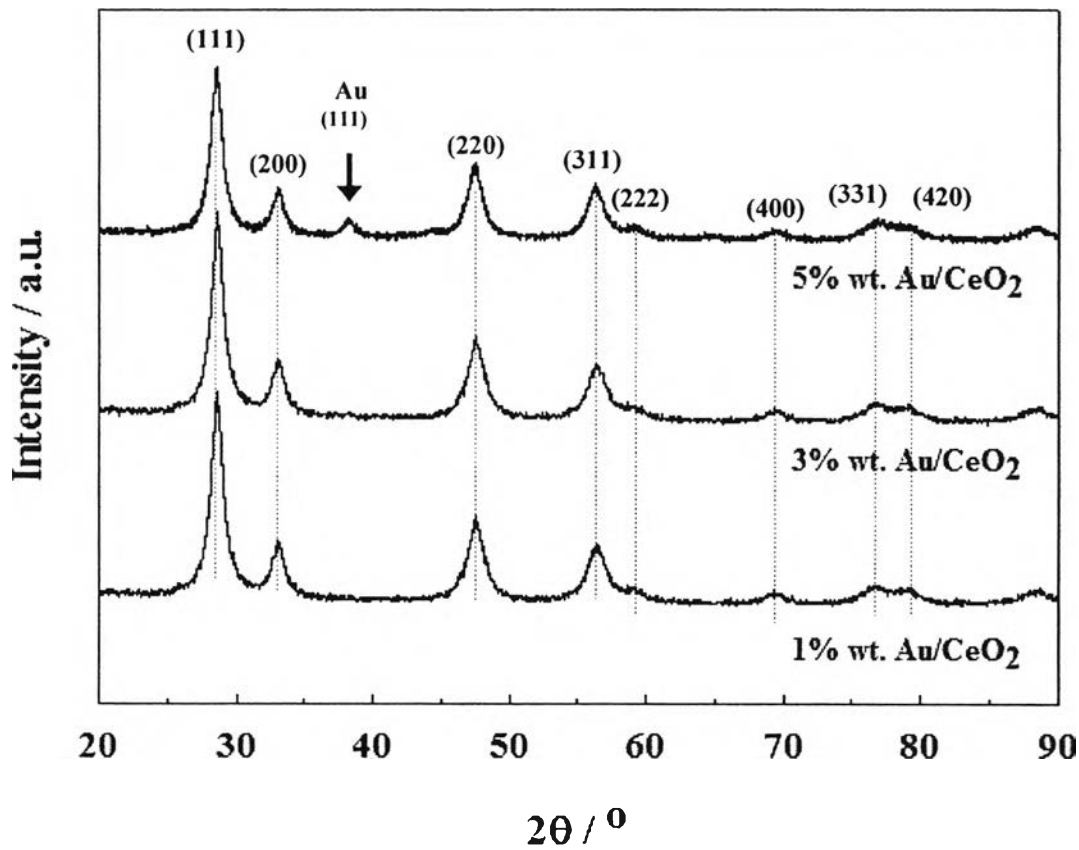

Figure 4.9 XRD patterns of the Au/CeO_2 catalysts with different Au loadings.

Table 4.3 Crystallite sizes of the Au/CeO_2 catalysts with different Au loadings

Catalysts	Crystallite size (nm.)				
	$CeO_2(111)$	$CeO_2(200)$	$CeO_2(220)$	$CeO_2(331)$	Au(111)
1%wt Au/CeO_2	11.20	14.73	17.15	36.01	<5
3%wt Au/CeO_2	13.25	15.82	11.85	30.04	<5
5%wt Au/CeO_2	13.49	17.53	11.01	40.87	9.38

From Table 4.3, the crystallinity of the CeO_2 decreased with increasing Au loading while the crystallite size of Au (111) increased to 9.38 nm, which is in agreement with many previous works that the increasing of Au metal could enhance the crystallinity of Au particle (Arena *et al.*, 2006).

4.1.3.3 Surface Area Measurement (BET)

The surface areas of 1%, 3%, 5%wt Au/CeO_2, and CeO_2 support are summarized in Table 4.4. After loading Au, the surface area of all catalysts decreased from 201.67 to 90.06 m^2/g. The variation of pore radius were approximately in the range of 44.24–48.68 Å for the more heavily loaded Au catalysts, probably attributed to blocking of the narrowest pores by the metal. However, the trends of surface areas were consistent with the XRD results. Some authors also observed the same results, which similar to this work (Jacobs *et al.*, 2005). In contrast to previous literature reviews, the increasing in crystallinity shown in XRD can lower the number of active sites of catalysts which corresponded to the decreasing in BET results (Perez *et al.*, 2008).

Table 4.4 BET surface areas of CeO_2, 1%, 3%, and 5%wt Au/CeO_2 catalysts

Catalyst	BET surface area (m^2/g)	Pore Radius (A°)
CeO_2 support	201.67	44.24
1% Au/CeO_2	118.43	41.92
3% Au/CeO_2	125.61	39.03
5% Au/CeO_2	90.06	48.68

4.1.3.4 Temperature-Programmed Reduction (TPR)

The temperature-programmed reduction (TPR) technique was used to study the reduction profiles of the catalysts. Figure 4.10 shows the TPR profiles of Au with different loadings. High surface area ceria usually have two distinct features in hydrogen TPR, a peak close to 800°C that is referred to the bulk reduction from CeO_2 to Ce_2O_3, and a broader peak situated close to 486°C that is typically assigned to a surface reduction process (Jacobs *et al.*, 2005). As has been noted in previous work, addition of metals can catalyze the surface reduction process, shifting the broad peak to lower temperatures, while not impacting bulk ceria reduction (Jacobs *et al.*, 2005). Yao and Yao (1984) indicated that surface

reduction probably involves the removal of surface capping oxygen atoms from ceria. For the Au reduction, the first peak reduction temperatures are close to 158°C, 113°C, and 124°C when Au loading were 1%, 3%, and 5%wt, respectively, corresponding to the reduction of Au_xO_y species (or Au hydroxide) to Au metal (Au^0). According to Fu *et al.* (2001), they analyzed that the presence of gold nanoparticles is the key for substantially weakening the surface oxygen of ceria and resulting its reduction temperature shifts to 100°C or lower. Interestingly, some authors have reported the relation between TPR and metal–support or metal–metal interaction linking with the catalytic activity. This is consistent with a detectable metal–support interaction between Au and ceria, which hinders the Au reduction at low loadings, where the strong interaction between metal and ceria would be higher. In the other words, it is important to better understand that the increasing of the loading can assist in decreasing metal–support interaction. This suggests that moving to a larger particle size for the more heavily loaded catalysts are more easily reduced to lower temperature (Jacobs *et al.*, 2005). This kind of phenomenon also referred to the presence of more Au metallic species for higher Au loading which can be detected by UV-vis spectra. It can be concluded that the high Au loading could lead to the high activity with the greatest Au metallic species and metal–metal interaction.

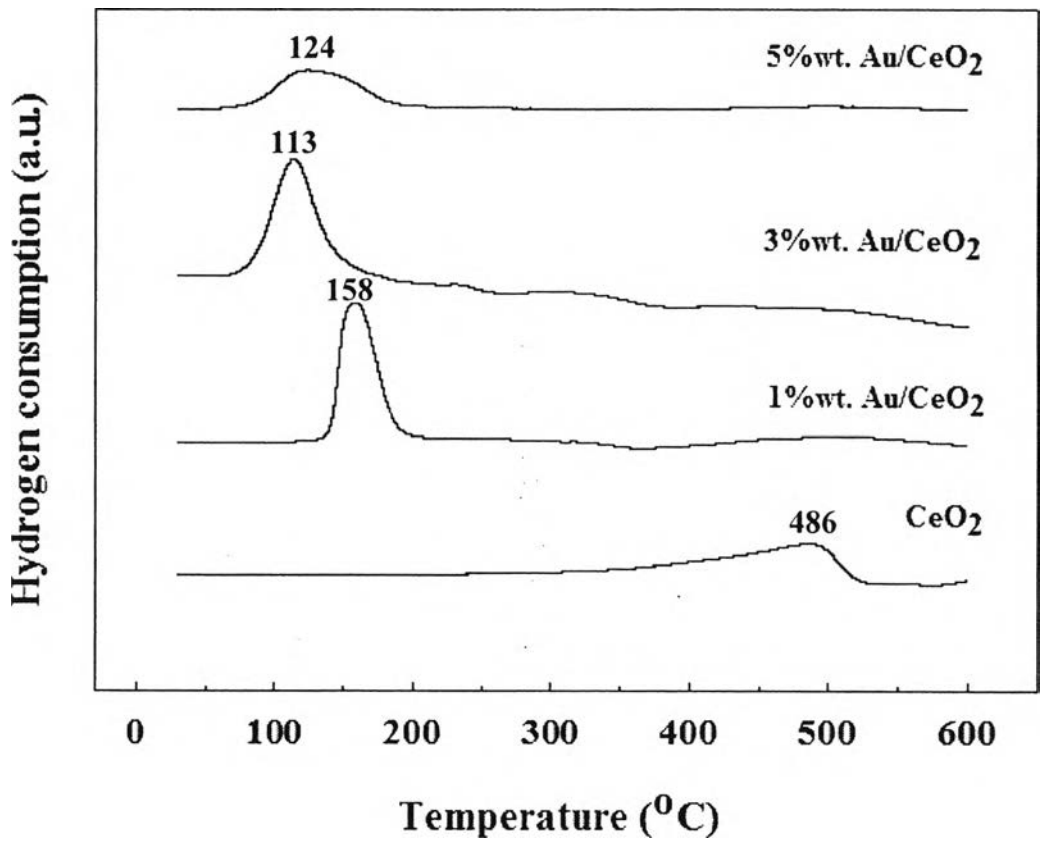

Figure 4.10 TPR profiles of Au/CeO_2 calcined at 400°C with different Au loadings.

4.1.3.5 UV-visible Spectroscopy

In recent years, there are many approaches to study the presence of small Au metal by using UV-vis spectroscopy to analyze gold species on the support. Normally, gold clusters (Au_n, $1 < n < 10$) can be observed at 280–380 nm (Park *et al.*, 2006). Absorptions at 550 and < 250 nm can be assigned to the gold nanoparticles (plasmon) (Zanella *et al.*, 2004) or Au metallic and Au^{3+} species, respectively (Souza *et al.*, 2008). However, the cerium oxide also shows bands in the range of 200–350 nm, as shown in Figure 4.11. Therefore, assigning Au^{3+} and gold clusters on Au/CeO_2 catalysts using UV-vis spectroscopy are impossible due to the interfering of combination of support and the resonance band of both gold species.

In the present work, all of samples showed the absorption band in the 500–600 nm region, which did not appear for the CeO_2 supports, related to the

gold metallic (plasmon) band. As it can be seen, the plasmon band was more pronounced when the Au loading was increased to 5%wt. According to Logunov *et al.* (1997), the Au with particle sizes less than 3 nm do not show a defined plasmon band clearly. In fact, these evidences were in line with the trends of XRD results which showed the Au peaks at high Au loading. In addition, these results also supported the TPR results that the highest Au loading represented the greatest metal–metal interaction leading to the formation of larger Au metallic particles which were obviously observed with the strongest band at 550 nm.

Nevertheless, the results did not support some literatures that the active non-metallic species are responsible for high activity in WGSR, although differences regarding preparation methods used among researchers may change the nature of active site (Jacobs *et al.,* 2005). For example, in certain cases, Au in a cationic state, strongly interacting with ceria, has been proposed to be an active center for WGSR. Au species with greater than zero oxidation state have been reported for catalyze the selective oxidation of CO (Guzman and Gates (2004)), as shown in almost metal oxide support. In contrast, Li-Hsin Chang and co-workers found that the active catalysts always contain metallic Au particles, while oxidic Au species are not responsible for steady-state high catalytic activity (Chang *et al.,* 2007). Moreover, Tuzovskaya *et al.* (2007) proposed that the co-existence of several types of active species of gold in CO oxidation having gold clusters < 1.5 nm are responsible for low-temperature activity and gold nanoparticles are responsible for high temperature activity. This could be an acceptable reason why the highest gold loading has the highest catalytic activity at high temperature ($\geq$ 200°C) for this study. However, the state of the gold in active catalysts is still unclear until now.

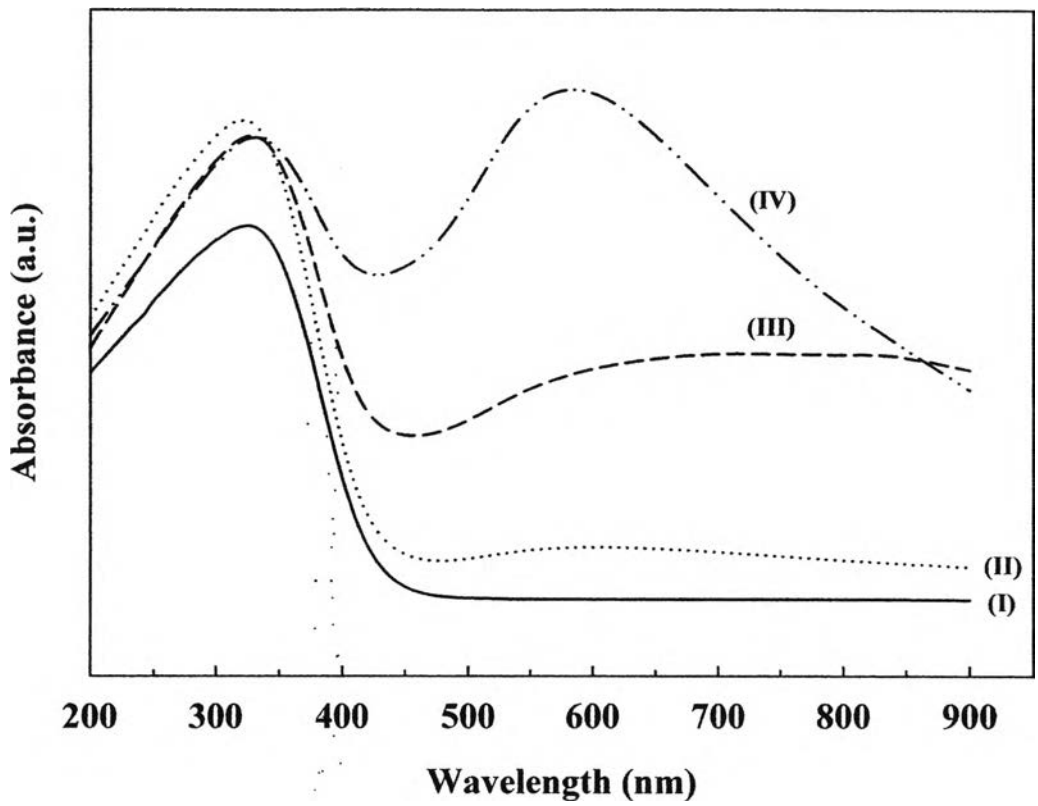

Figure 4.11 Diffuse Reflectance UV–vis spectra of Au species calcined at 400°C with different Au loadings. (I) CeO_2 support; (II) 1%wt Au/CeO_2; (III) 3%wt Au/CeO_2; (IV) 5%wt Au/CeO_2.

4.1.3.6 Transmission Electron Microscope (TEM)

Figure 4.12 shows the TEM images of the Au/CeO_2 calcined at 400°C with different Au loading; 1%, 3%, and 5%wt. The Au particles can be seen as dark spot on the supports. The mean particle size of Au of 1%, 3%, and 5%wt were 2.82, 4.86, and 10.04 nm, respectively. The 5%wt Au/CeO_2 catalyst has the largest Au particle sizes when compared to the various loadings at 3% and 1%. This phenomenon agrees with the activity testing and previous characterization results. The more metal loading in the catalysts, the more larger of Au particle than others. Consequently, it can be concluded that the 5%wt Au/CeO_2 represents the highest activity because of the presence of the largest gold metallic sizes playing a significant role for the activity in OSRM.

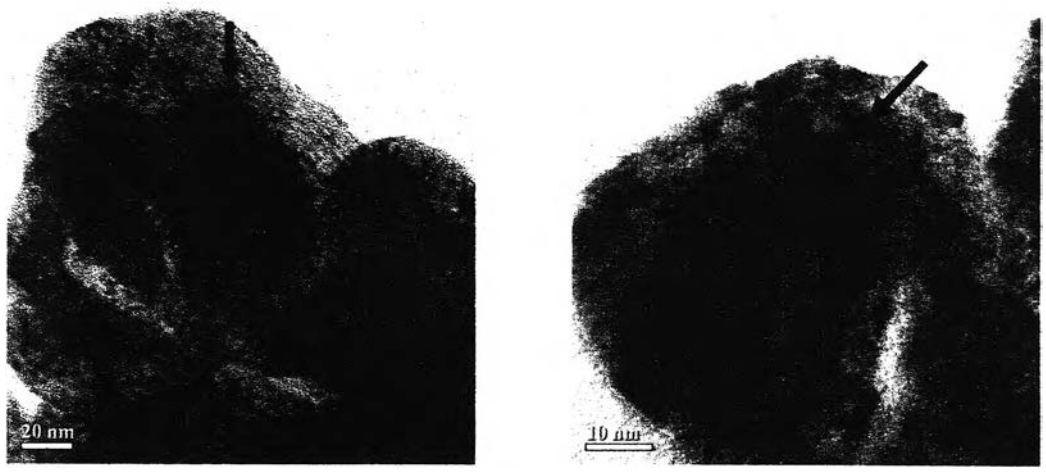

a) 1%wt Au/CeO_2

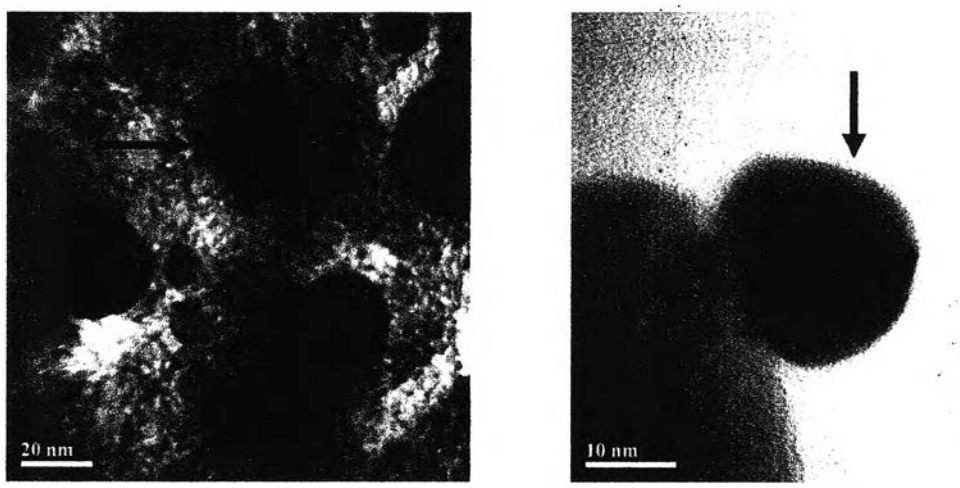

b) 3%wt Au/CeO_2

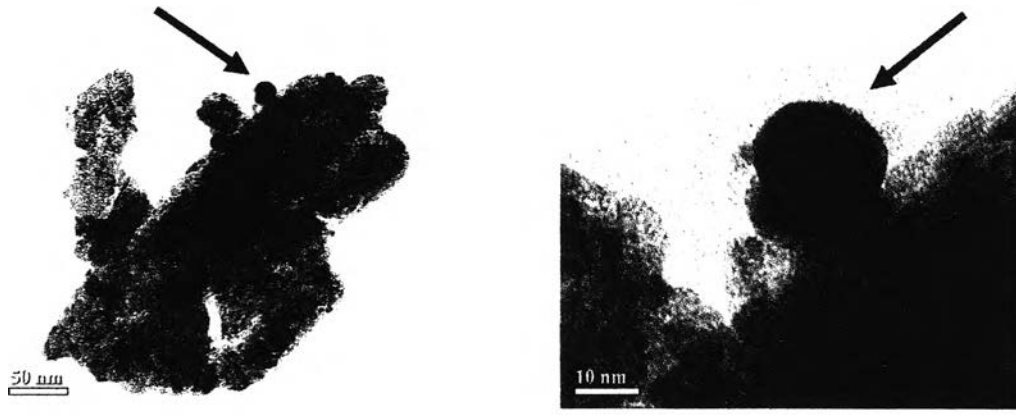

c) 5%wt Au/CeO_2

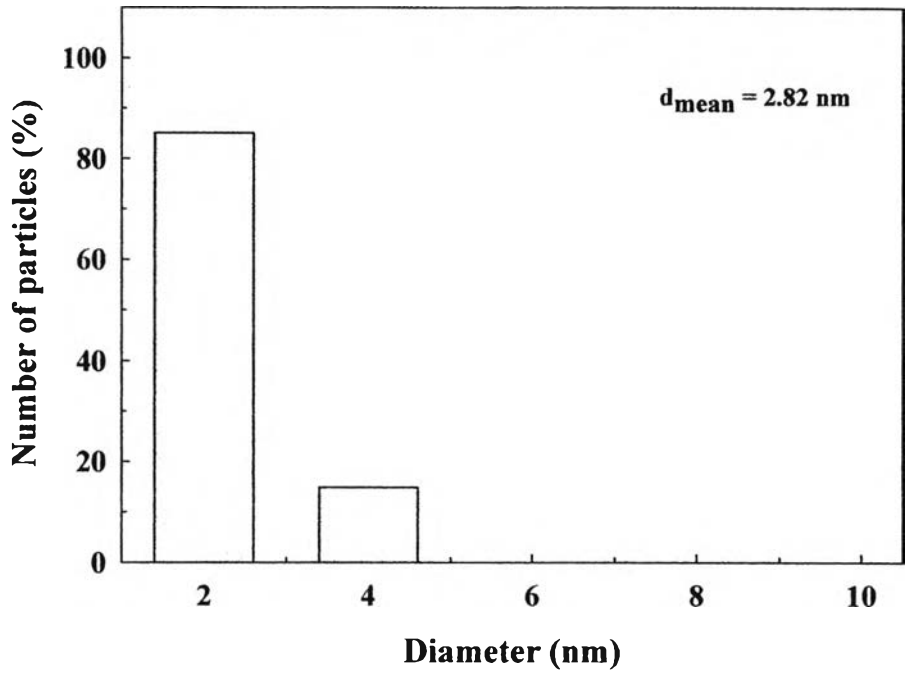

a) 1%wt Au/CeO_2

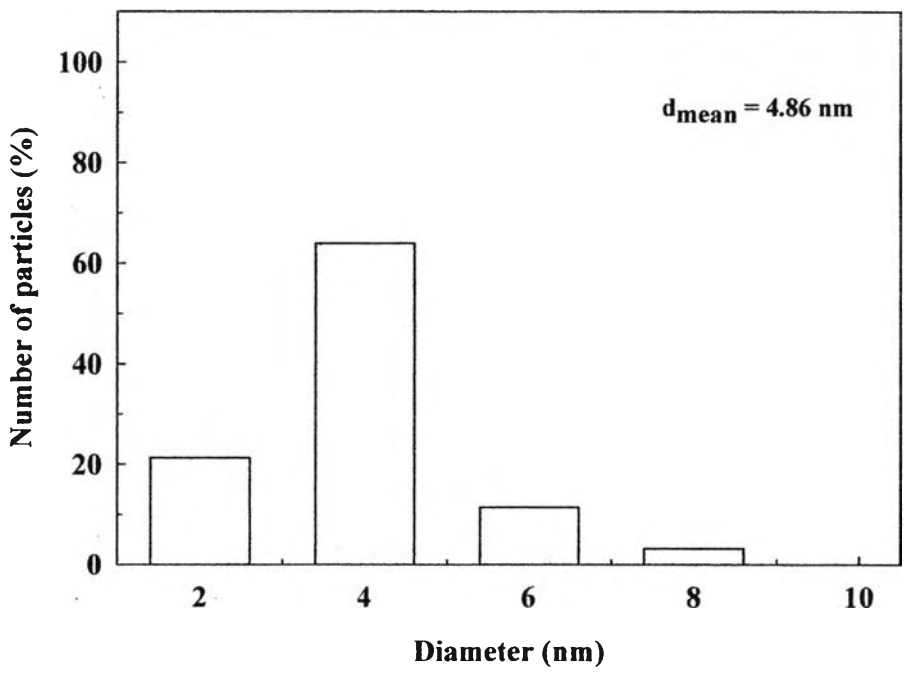

b) 3%wt Au/CeO_2

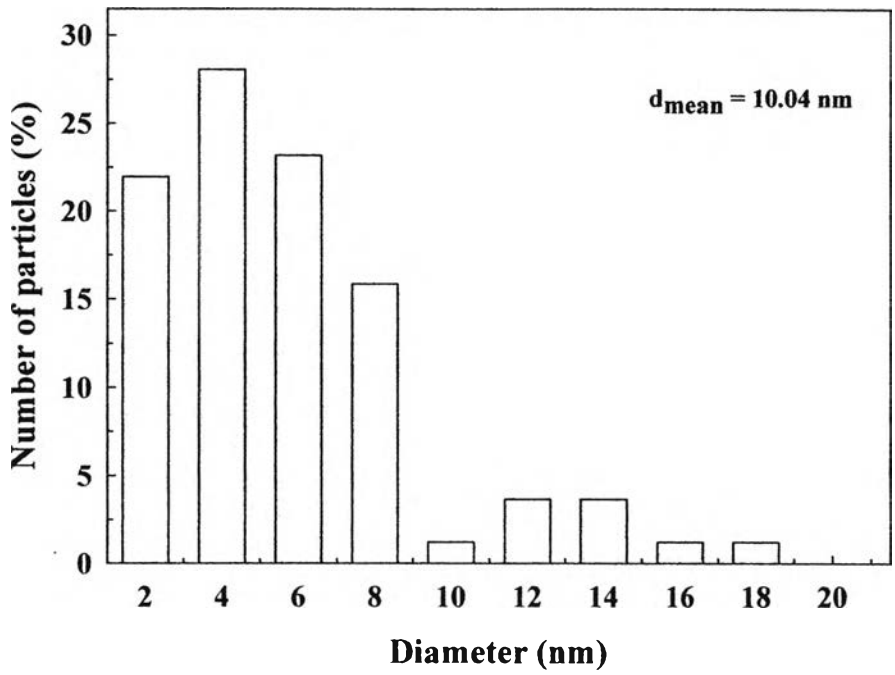

c) 5%wt Au/CeO_2

Figure 4.12 TEM images and particle size distribution of Au/CeO_2 catalysts with different Au loadings.

4.1.4 Effect of Calcination Temperature on the Catalytic Performance

The behavior of 5%wt Au/CeO_2 catalysts shown in Figures 4.13–4.14 can be explained by considering the calcination temperature. The prepared catalysts were calcined in air at different temperatures (300, 400, 500, and 600°C) for 4 hours.

Both methanol conversion and hydrogen yield (Figure 4.13) were strongly influenced by the negative effect of low calcination temperature at 300°C while the highest catalytic activity—methanol conversion almost 100% and the highest hydrogen yield at 23.52%—was obviously observed in the calcination temperature of 400°C in the range of low temperature (200–300°C). With increasing the calcination temperature, the OSRM decreased due to the decrease in surface area since the catalyst would undergo a little bit phenomenon of sintering. To better understand the cause of agglomeration occurred at high calcination temperatures, this effect might be attributed to the particles coalescence with TEM results. Figure 4.14 illustrates that the CO, CO_2, and CH_4 selectivity did not immensely differ with the

previous effect (Au loading effect) during the OSRM reaction for all calcination temperatures.

For the initial results, it could be concluded that the appropriate calcination temperature was 400°C for the catalyst preparation.

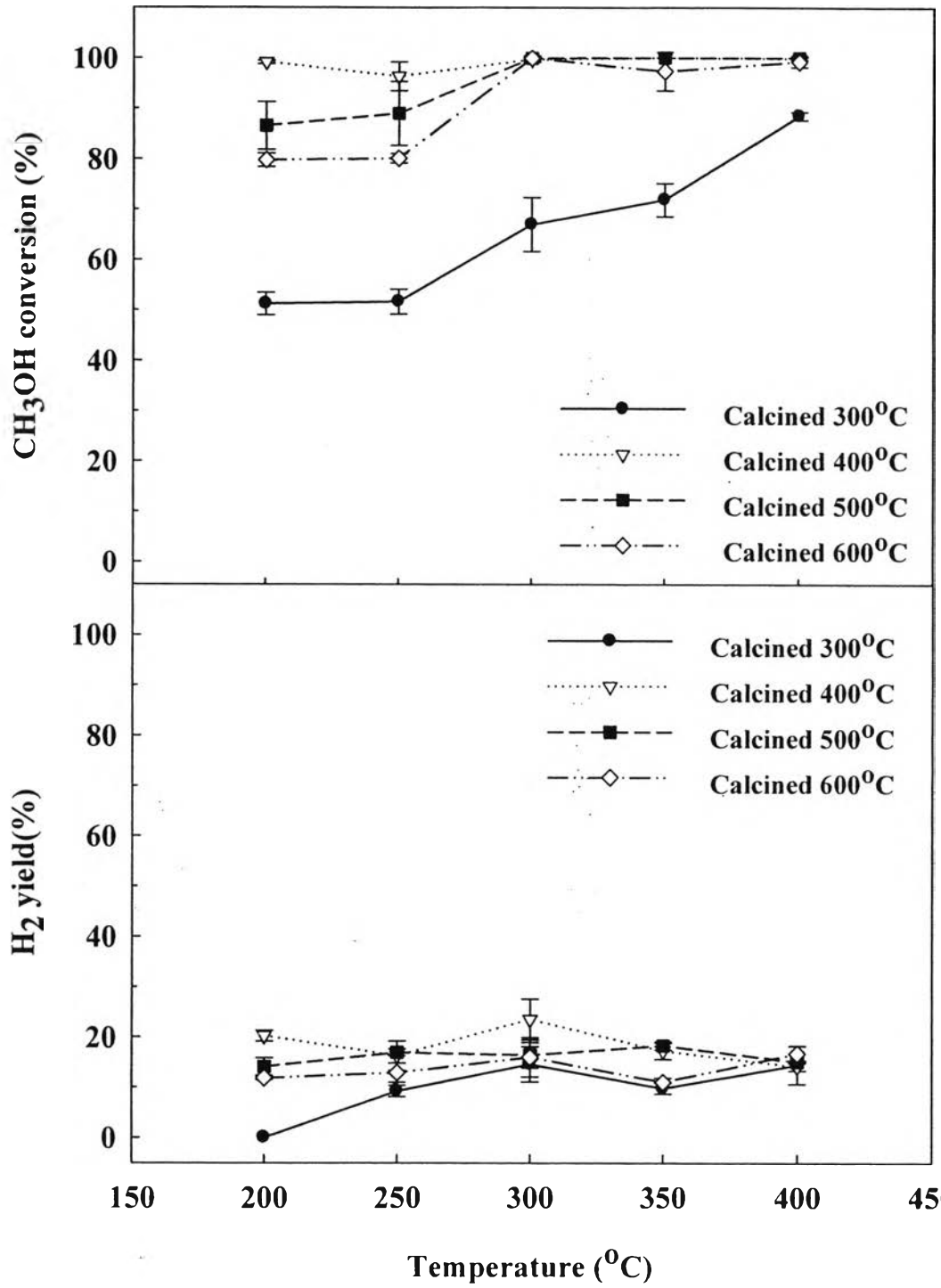

Figure 4.13 Effect of calcination temperature on methanol conversion and hydrogen yield over 5%wt Au/CeO_2. Reaction condition: $O_2/H_2O/CH_3OH$ = 1.25/2/1.

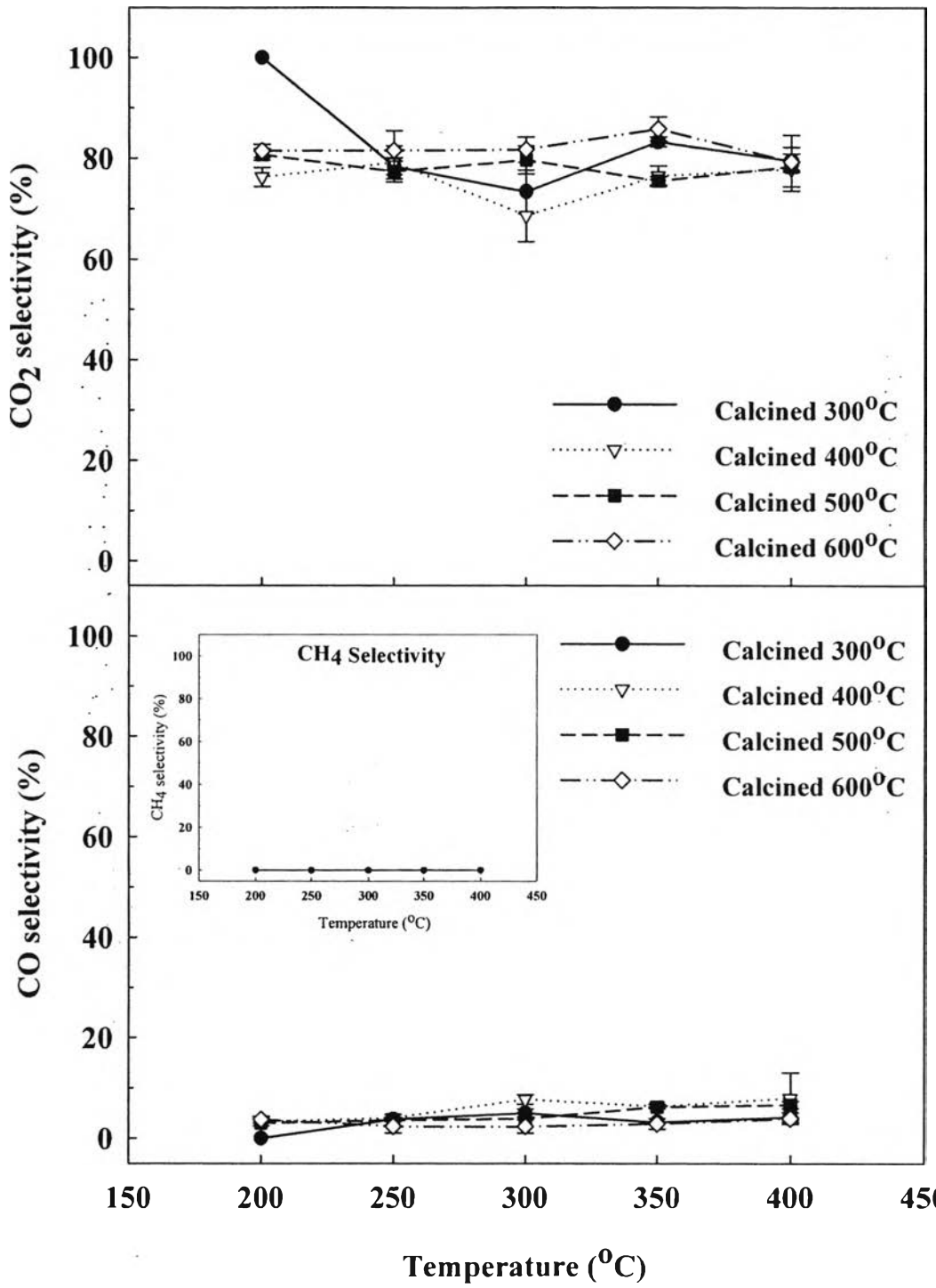

Figure 4.14 Effect of calcination temperature on CO_2, CO, and CH_4 selectivity over 5%wt Au/CeO_2. Reaction condition: $O_2/H_2O/CH_3OH$ = 1.25/2/1.

4.1.4.1 Atomic Absorption Spectroscopy (AAS)

In order to analyze the actual metal loading of 5%wt Au/CeO_2 catalysts with various calcination temperatures, AAS technique was used and the results are summarized in Table 4.5.

Table 4.5 AAS of 5%wt Au/CeO_2 with various calcination temperatures

Catalysts	Actual metal loading (%wt.)
calcined at 300°C	4.37
calcined at 400°C	4.42
calcined at 500°C	5.11
calcined at 600°C	4.86

4.1.4.2 X-ray Diffraction (XRD)

From Figure 4.15, it is clearly seen that the appearance of Au(111) reflection becomes more visible when increasing the calcination temperature higher than 400°C. In contrast, there was no significant difference in every crystallite planes of CeO_2. This is in line with Li-Hsin Chang *et al.* (2007) that the crystallite size of Au/CeO_2 increased with increasing calcination temperature. Interestingly, the appearance of Au(200) and Au(220) reflections becomes more visible after calcination at 500°C. The appearance of gold reflection at higher temperature may be attributed to the agglomeration of gold particles. In other words, it is interpreted as due to a higher average gold particle size. Feg-Wen Chang *et al.* (2005) also reported that the Au(200) plane appeared after calcination at 400°C because of its larger gold particle size. Eun and Jae (1998) have discussed about the effect of calcination temperature on Au particle size in Au/Fe_2O_3 that the catalytic activity decreased as the calcination temperature increased since the particle size of the metallic gold became larger with increasing calcination temperature.

According to the Scherrer equation, the crystalline sizes of gold and ceria were calculated and summarized in Table 4.6 (Au(200) wasn't shown

for this case.). However, the gold particle size could not be determined accurately from the line of the gold reflections. The TEM technique was subsequently used to evaluate the size of the reduced gold particles.

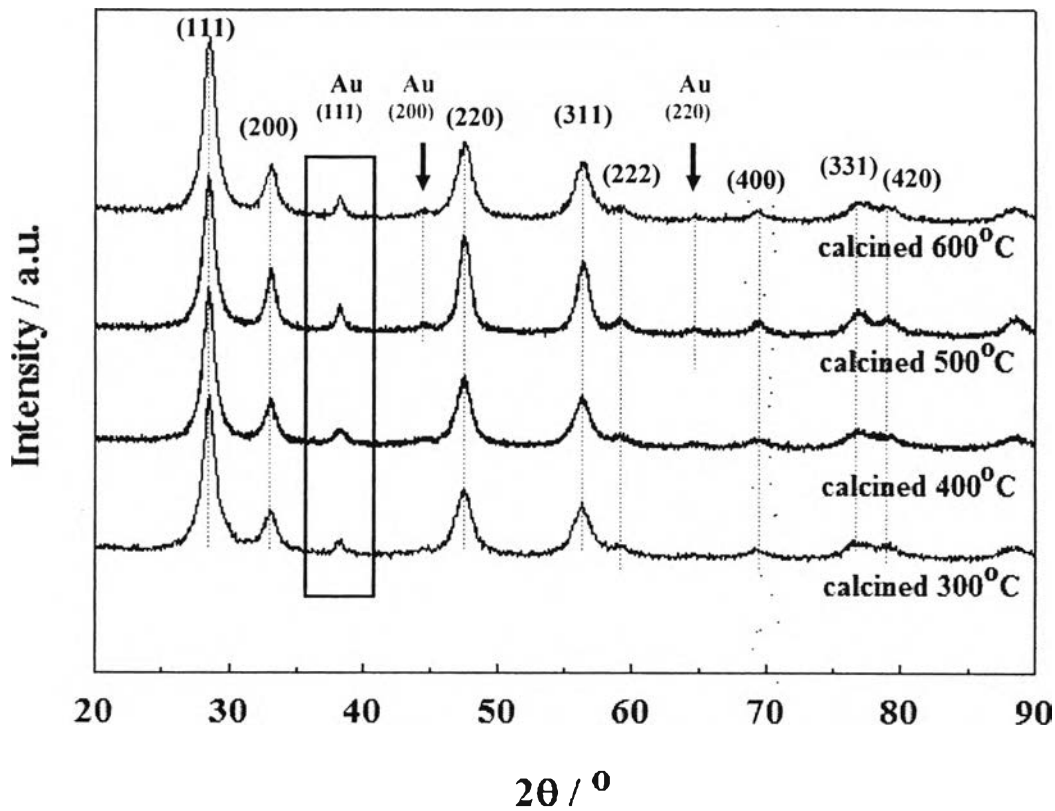

Figure 4.15 XRD patterns of Au/CeO_2 catalysts with various calcination temperatures.

Table 4.6 Crystallite sizes of the Au/CeO_2 with various calcination temperatures

Catalysts	Crystallite size (nm.)					
	$CeO_2(111)$	$CeO_2(200)$	$CeO_2(220)$	$CeO_2(331)$	Au(111)	Au(220)
calcined at 300°C	9.18	10.51	8.57	22.43	16.62	< 5
calcined at 400°C	13.49	17.53	11.01	40.87	9.38	< 5
calcined at 500°C	13.01	13.64	10.42	40.91	21.33	27.83
calcined at 600°C	9.72	8.66	8.12	36.08	24.84	37.95

4.1.4.3 Surface Area Measurement (BET)

The surface areas of 5%wt Au/CeO_2 with various calcination temperatures are summarized in Table 4.7. The surface area directly decreased with increasing calcination temperature from 125.71 m^2/g (300°C) to 68.51 m^2/g (600°C). The variation of pore radius was approximately in the range of 41.60–62.24 Å for high calcination temperature. Nevertheless, the trends of surface areas were also in line with the XRD results that the high calcination temperature strongly affected the sintering of gold particle resulting in larger particle size. It can also be noted that the large particle size of metallic Au can easily lower catalytic activity (Eun *et al.*, 1999).

Table 4.7 BET surface areas of 5%wt Au/CeO_2 catalysts with various calcination temperatures

Catalyst	BET surface area (m^2/g)	Pore Radius (Å)
calcined at 300°C	125.71	41.60
calcined at 400°C	90.06	48.68
calcined at 500°C	74.68	60.77
calcined at 600°C	68.51	62.24

4.1.4.4 Temperature-Programmed Reduction (TPR)

As shown in Figure 4.16, it can be obviously observed that the increasing of calcination temperature doesn't seem to improve the metal-metal interaction and metal-support interaction in 5%wt Au/CeO_2 because of the slight difference in reduction temperature of Au_xO_y, which is approximately in the range of 112–133°C. Similar to the previous section, the temperature reduction of bulk ceria also strongly pronounced in two peaks—800°C that is referred to the bulk reduction from CeO_2 to Ce_2O_3, and a broader peak situated close to 486°C that is typically assigned to a surface reduction process (Jacobs *et al.*, 2005). To explain the catalytic activity in this effect, the other characterized results could be required to solve the problems.

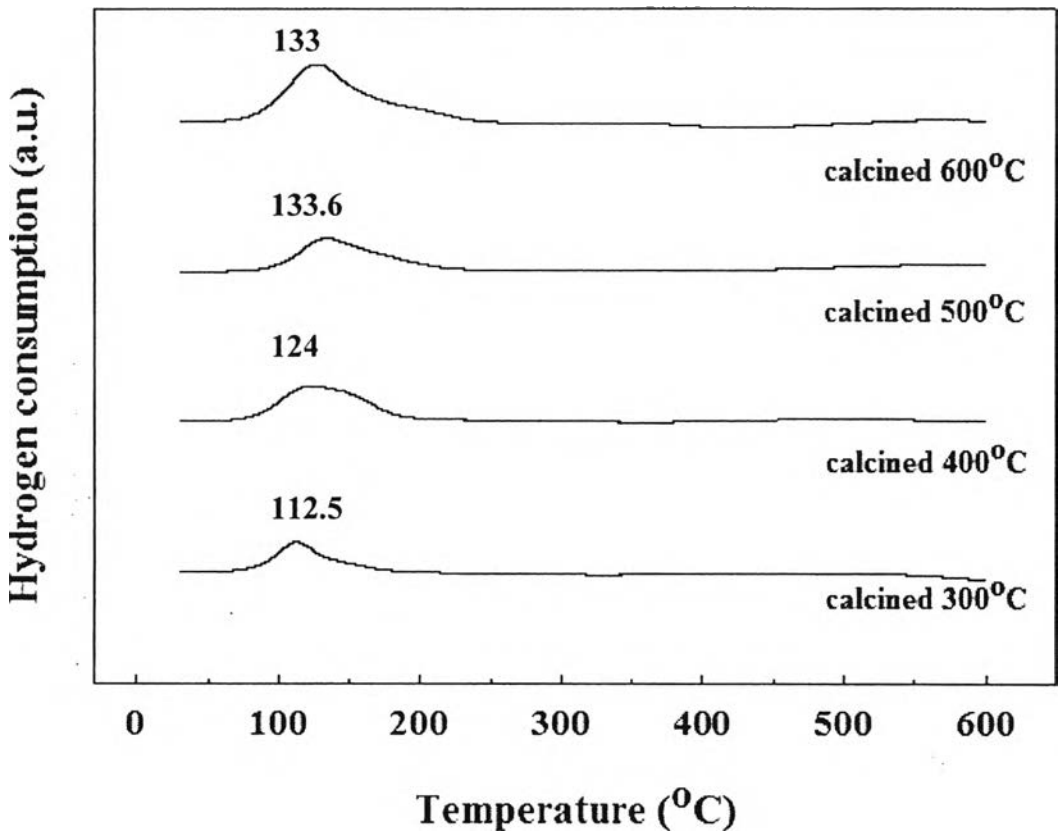

Figure 4.16 TPR profiles of Au/CeO_2 calcined with various calcination temperatures.

4.1.4.5 UV-visible Spectroscopy

According to the Figure 4.17, the catalytic activities of the catalysts calcined at 300°C and 400°C and the presence of Au metallic particle or Au^0 specie at 550 nm could be related. The catalyst calcined at 400°C exhibited the highest catalytic performance together with the highest amount of Au^0 specie. It can be implied that the more Au^0 species played an important role with higher catalytic performance for calcination temperature of 400°C. Furthermore, the positive effect of thermal treatment is mainly to reduce the oxidation state of Au^{3+} to Au^0 for being the active sites (Bond *et al.*, 2006). Until now, the correlation between the gold oxidation state or gold phase and the calcination temperature has been reported that the gold phase was changed from $Au(OH)_3$ or Au_2O_3 to metallic Au as the calcination temperature increased (Eun *et al.*, 1999). In contrast, El-Moemen *et al.*

(2008) proposed that the highest activity of WGSR has been observed with the lowest amount of Au^{3+} and the highest amount of Au^0. However, it still be implied that cationic gold species were inactive by themselves, but were necessary in combination with Au^0 to obtain activity (Bond *et al.*, 2006). For the catalysts calcined at 500°C and 600°C, the decreasing in an active surface area of the catalysts was observed since the catalysts would undergo a little bit phenomenon of sintering which was the only possibility for explaining this occurrence. As prediction, the Au^0 must be higher with increasing calcination temperature, similar to many previous literature reviews. Conversely, the intensities of Au^0 species of catalysts calcined at 500°C and 600°C turned to decrease significantly. It has been reported in previous literature that the effect of heat treatment over Au/CeO_2 catalysts (Bera and Hegde (2002)), which demonstrated that the performance of CO oxidation of Au/CeO_2 catalysts, decreased with increasing the concentration of Au^{3+} species by heated at 800°C while our experiments could not detect the appearance of Au^{3+} with UV-vis technique since the overlap between Au^{3+} species and CeO_2 support for every calcination temperatures. Moreover, Smolentseva E. and coworkers found that the contribution of the gold nanoparticles or Au^0 species increased with calcination temperature while our experiments were not the same trend with metallic Au (Smolentseva *et al.*, 2006).

However, it should be strongly recommended that the catalytic performance depended on the preparation technique during the experiment. To better understand the cause of agglomeration occurred at high calcination temperature, this effect might be attributed to the particles coalescence with TEM results. Figure 4.14 illustrates that the CO, CO_2, and CH_4 selectivity did not immensely differ with the previous effect (Au loading effect) during the OSRM reaction for all calcination temperatures.

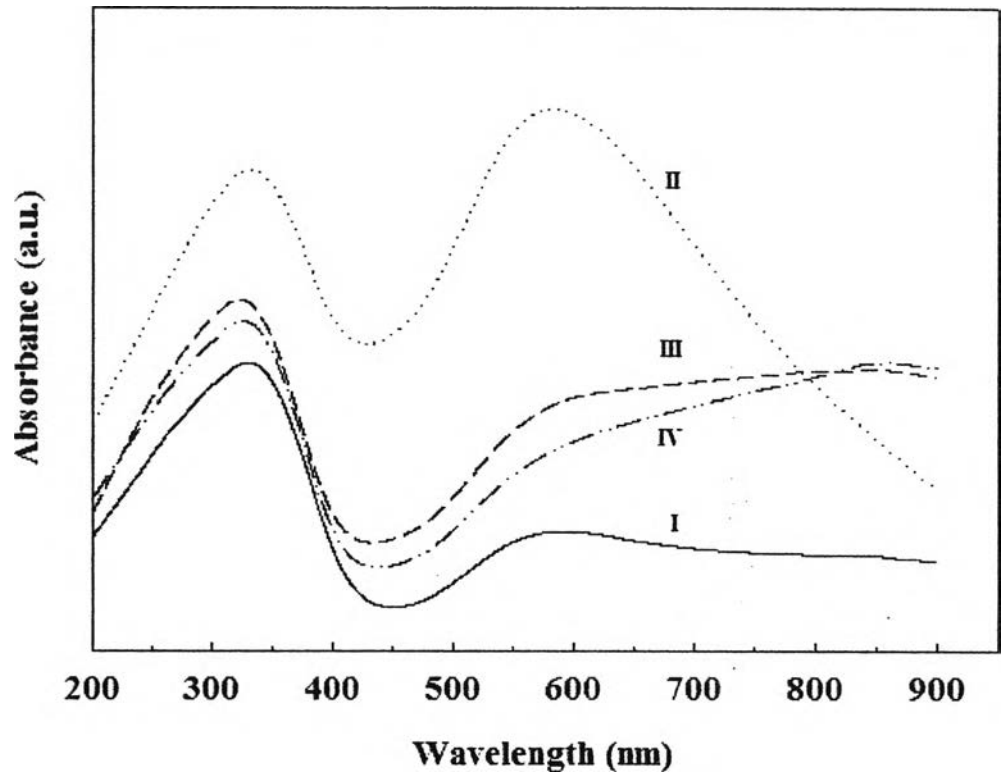

Figure 4.17 Diffuse Reflectance UV–vis spectra of 5%wt Au/CeO_2 with different calcination temperatures. (I) calcined at 300°C; (II) calcined at 400°C; (III) calcined at 500°C; (IV) calcined at 600°C.

4.1.4.6 Transmission Electron Microscope (TEM)

Figure 4.18 shows the TEM images of the 5%wt Au/CeO_2 with various calcination temperatures. The mean particle size of Au with various calcinations temperatures of 300, 400, 500, and 600°C were 43.30, 10.04, 44.85, and 51.93 nm, respectively. The catalyst calcined at 600°C has the largest Au particle size when compared to others. This phenomenon agrees with the existence of sintering according to lower catalytic activity. In contrast, the catalyst calcined at 400°C shows the lowest Au particle size which might be the optimum size for the OSRM reaction. Therefore, it can be concluded that the suitable calcination temperature was 400°C.

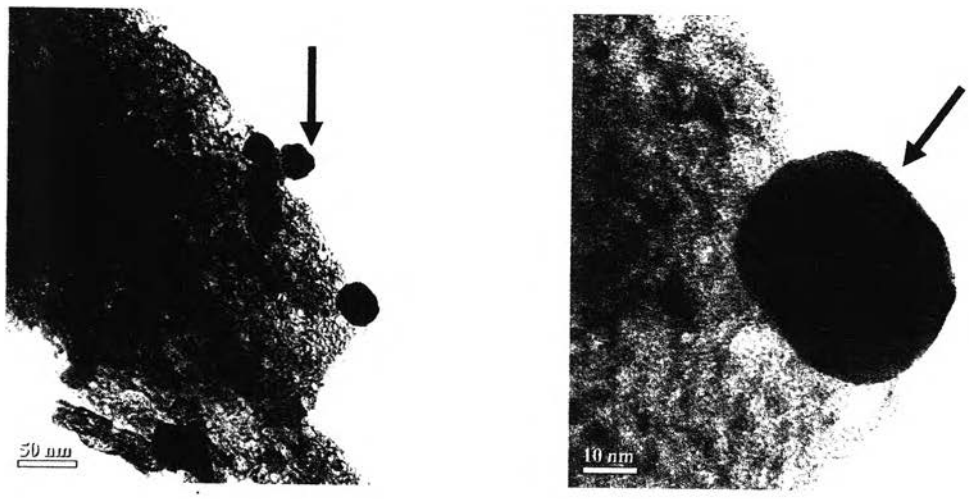

a) Calcined at 300°C

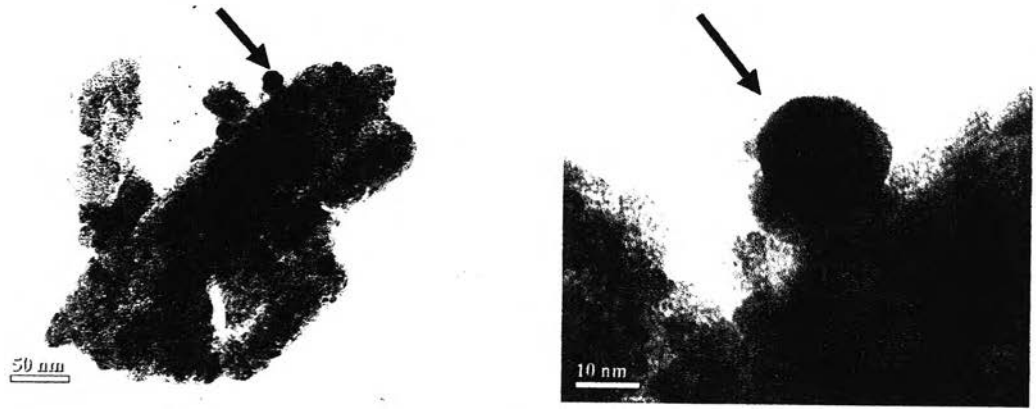

b) Calcined at 400°C

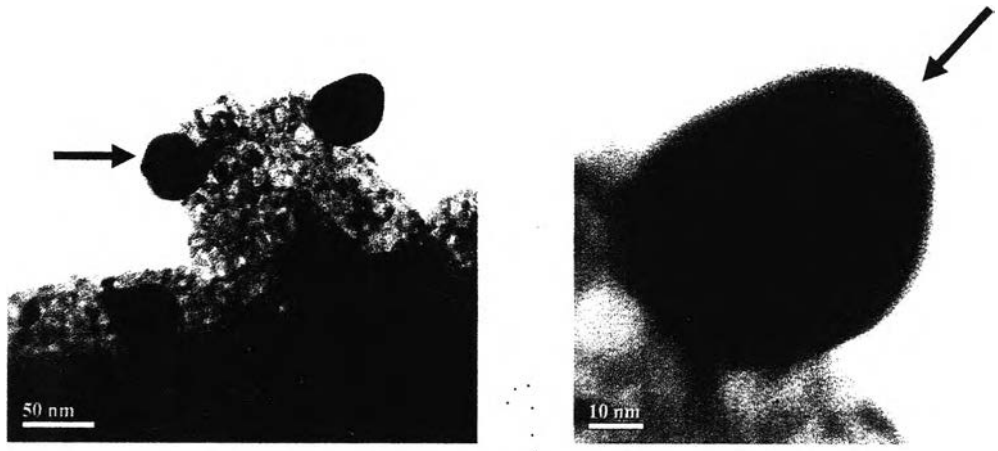

c) Calcined at 500°C

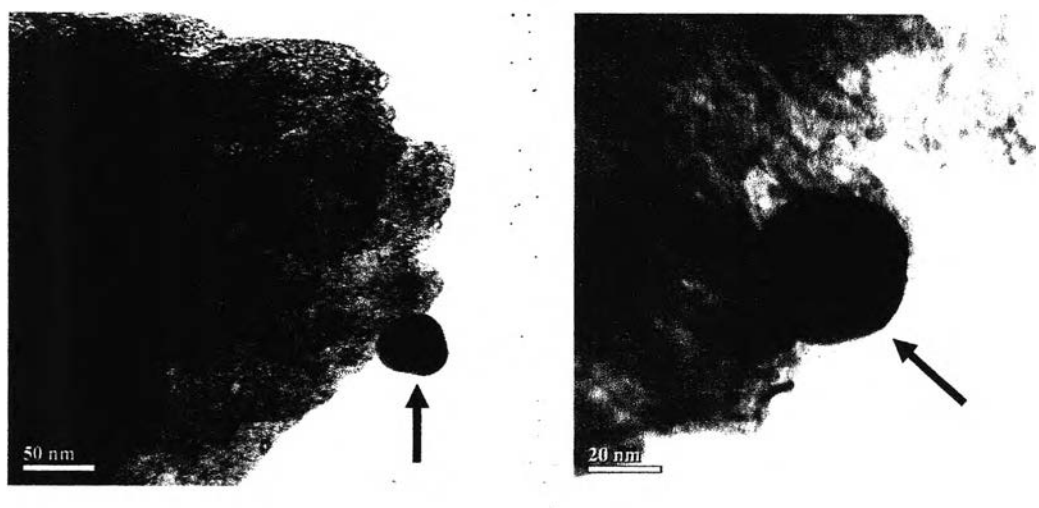

d) Calcined at 600°C

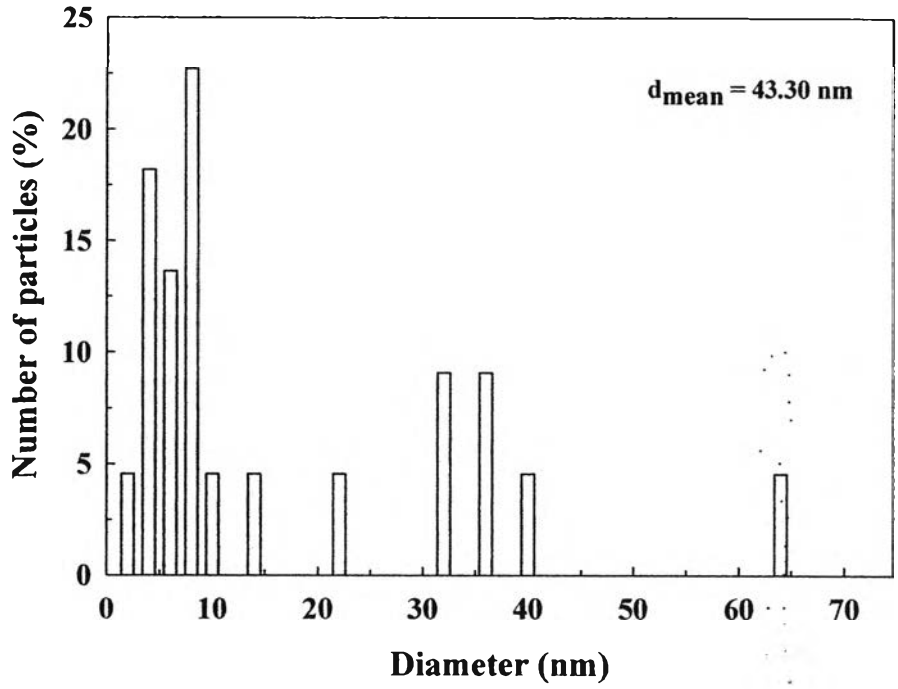

a) Calcined at 300°C

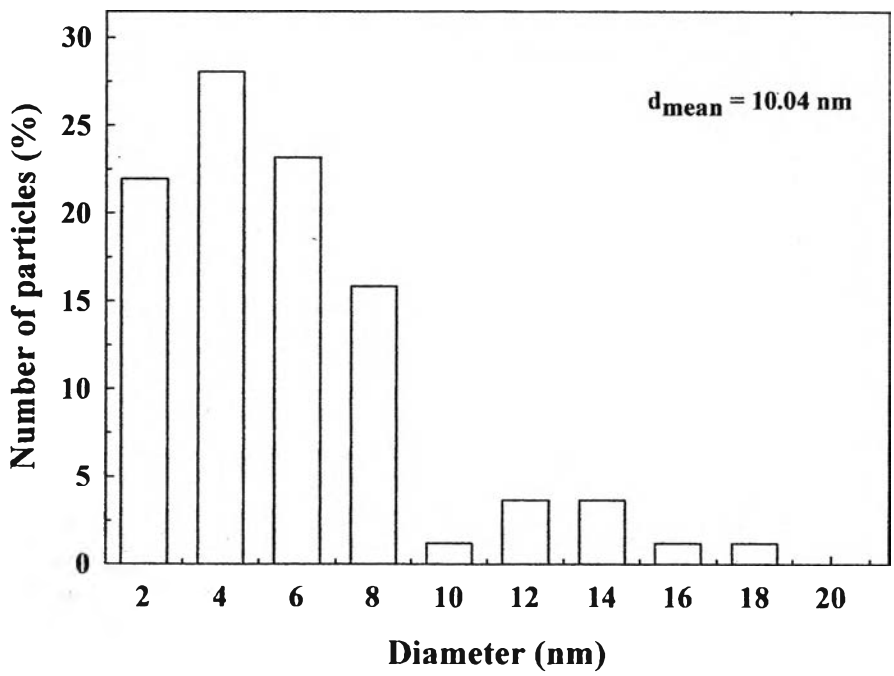

b) Calcined at 400°C

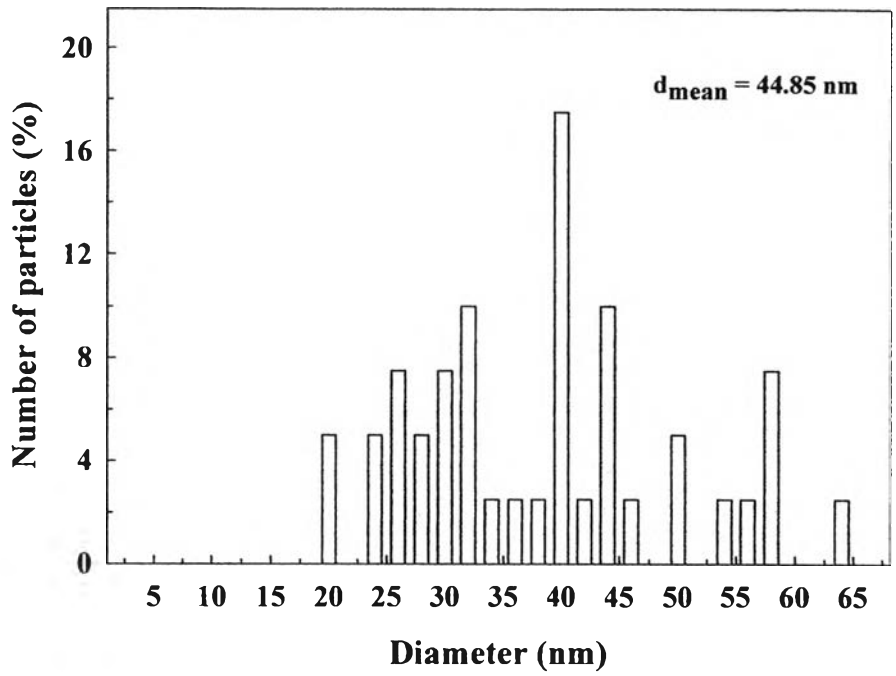

c) Calcined at 500°C

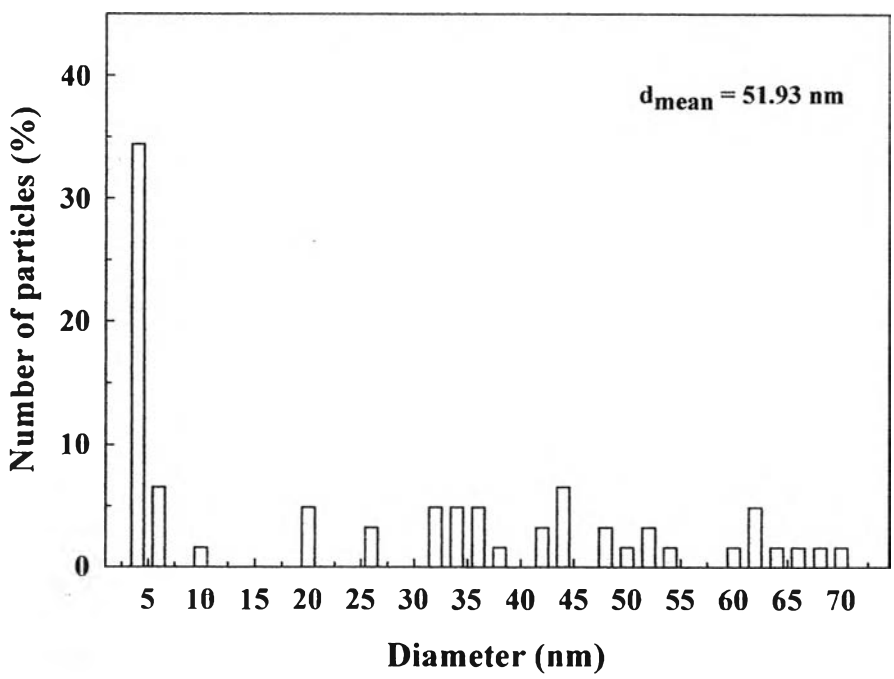

d) Calcined at 600°C

Figure 4.18 TEM images and particle size distribution of Au/CeO_2 catalysts with various calcination temperatures.

4.1.5 Comparison of Catalytic Performance between Support and Supported Au Catalysts

To evaluate the catalytic behavior of the prepared catalysts with and without metal loading, the 5%wt Au/CeO_2 and CeO_2 catalysts calcined at 400°C were compared for the OSRM reaction at the $O_2/H_2O/CH_3OH$ molar ratio at 1.25/2/1 in the temperature range of 200 to 400°C.

As illustrated in Figure 4.19, the gap differences in methanol conversion and hydrogen yield between 5%wt Au/CeO_2 and CeO_2 were large. As expected, the Au-based catalyst was responsible for the high catalytic activity in the whole range of reaction temperature. In contrast, the CeO_2 as a support has no activity at the same range of reaction temperature. It can be concluded that Au plays the major role as the active site for the OSRM.

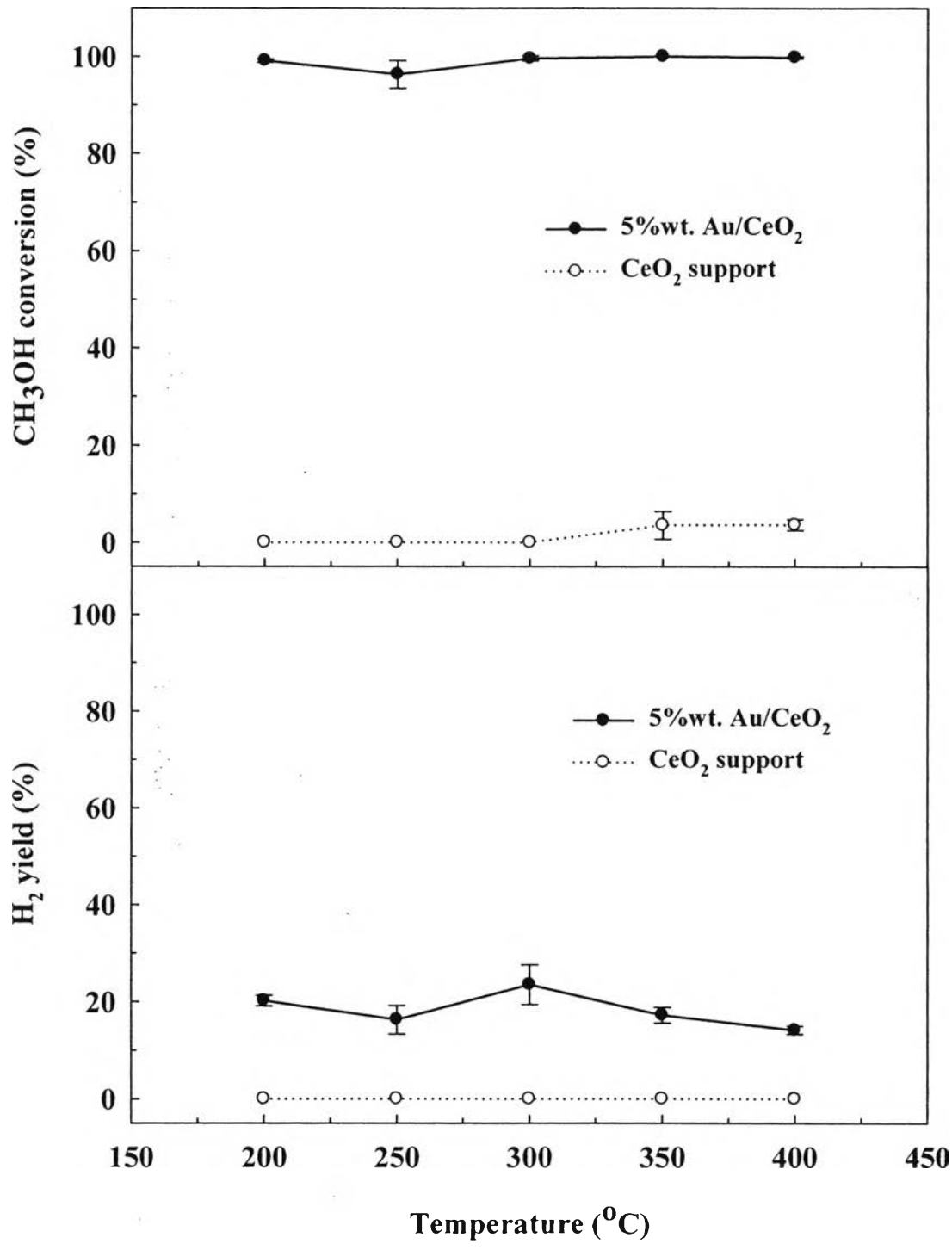

Figure 4.19 Comparison between the catalytic activity of CeO_2 support and 5%wt Au/CeO_2 catalyst calcined at 400°C. Reaction condition: $O_2/H_2O/CH_3OH$ = 1.25/2/1.

4.2 Deactivation and Side reactions (DCM, WGSR, and POM)

From previous section, the 5%wt Au/CeO_2 calcined at 400°C showed the highest catalytic activity. In this part, the 5%wt Au/CeO_2 was performed in the methanol decomposition, partial oxidation, and water gas shift reaction, respectively, to study the catalytic performance in three side reactions involving with hydrogen production. In addition, the stability of this catalyst was carried out for 1 week (168 hours).

4.2.1 Deactivation Test

In order to check the stability of the prepared catalyst at constant temperature, the prepared catalysts were carried out at the $O_2/H_2O/CH_3OH$ molar ratio 1.25/2/1 under atmospheric pressure for 168 hours. The 5%wt Au/CeO_2 catalyst calcined at 400°C, which showed the maximum methanol conversion and H_2 selectivity, was tested at the constant operating temperature of 300°C, as shown in Figure 4.20. It can be seen that the methanol conversion dropped rapidly to 88.8% after 40 hours, and then stayed steadily at the approximate value of 87.2%. This corresponded to the stability of Au/CeO_2 catalysts which could be stable almost 100% conversion for the initial time of experimental test. Nevertheless, the average trend of H_2 yield at 16.12% was still unclear due to the fact that the existence of side reactions might dominate the hydrogen production instead of OSRM reaction during the time of experimental test. This also led to an unstable of the selectivity of each product gas with free methane formation. The average values of H_2, CO, and CO_2 selectivity were presented at 17.85%, 12.57%, and 69.58%, respectively. As can be seen, we speculate that our catalyst was still the long term stable catalyst due to the fact that it still gave the high scale of methanol conversion and the stable hydrogen yield in the whole time on stream.

Generally, both sintering of the catalysts and coke formation might occur during the SRM. During the deactivation, the accumulation of the unreformed hydrocarbons due to the low conversion would lead to an increased probability of having coke formation on the catalyst surface (Lin *et al.*, 2007). To confirm the

existence of these effects, TPO and XRD were used to identify the coke formation and the sintering of the spent catalyst after the stability test.

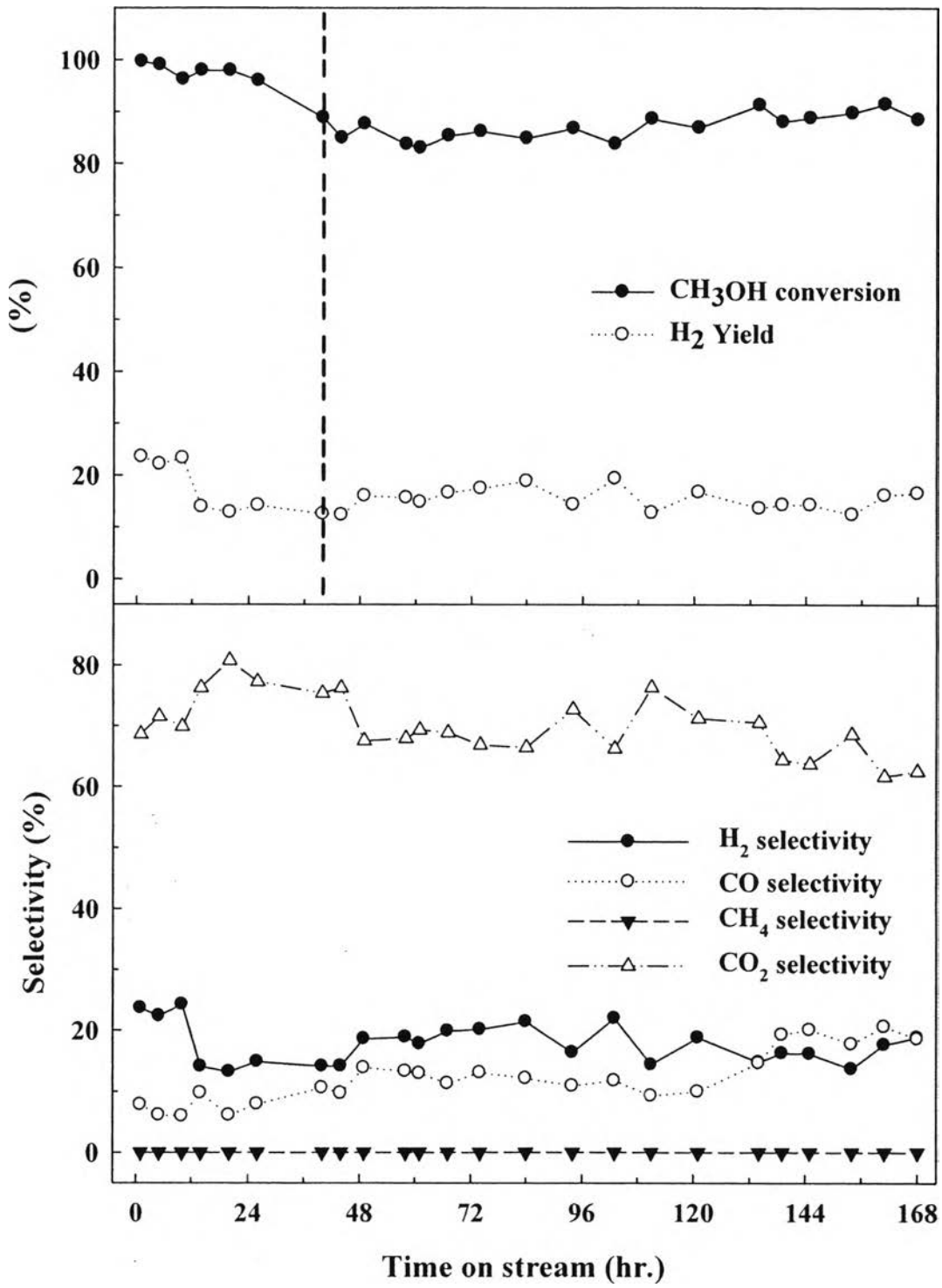

Figure 4.20 Deactivation test of 5%wt Au/CeO_2 catalyst calcined at 400°C. Reaction conditions: $O_2/H_2O/CH_3OH$ = 1.25/2/1, reaction temperature of 300°C, and time on stream = 168 hours.

4.2.1.1 Temperature-Programmed Oxidation (TPO)

Temperature-programmed oxidation (TPO) technique was widely used to measure the amount of coke or carbon deposited on the spent catalyst. As illustrated in Figure 4.21, the TPO profiles of the spent catalyst of 5%wt Au/CeO_2, which was carried out at the reaction temperature of 300°C for 168 hours, involves two peaks of coke—the first low temperature peak with high intensity at 274°C and the second high temperature peak with low intensity at 502°C—implying at least two types of carboneous species were formed. Guisnet and Magnoux (2001) have proposed the overview about the classification of coke formation on catalyst surface depending on the reaction temperature and the type of reaction. For the low reaction temperature (<200°C), the coke deposited was not polyaromatic type. At high temperature (>350°C), the coke components were polyaromatic type. Additionally, the difference in peak positions indicated the interaction between each type of coke deposited on the surface of catalyst and the support. The first type could be assigned to the oxidation of the poorly polymerized coke deposited on the metal particles and the second type represented the high polymerized coke deposited near the metal-support interphase (Luengnaruemitchai *et al.*, 2008). The amount of coke deposited on the spent catalyst was measured approximately at 0.75%wt. Consequently, the rate of carbon formation could be calculated and given at 1.031E-09 mole C/sec-g_{cat}. It should be noted that the amount of coke deposited on the metal is higher than that on the support. Faungnawakij *et al.* (2006) has reported that CO could be the source of coke formation or carbonaceous deposition. To support this appearance, Armor *et al.* (2008) proposed the major pathways for coke formation. As a result, it could be concluded that the coke formation does not affect dramatically the catalytic activity of the catalyst.

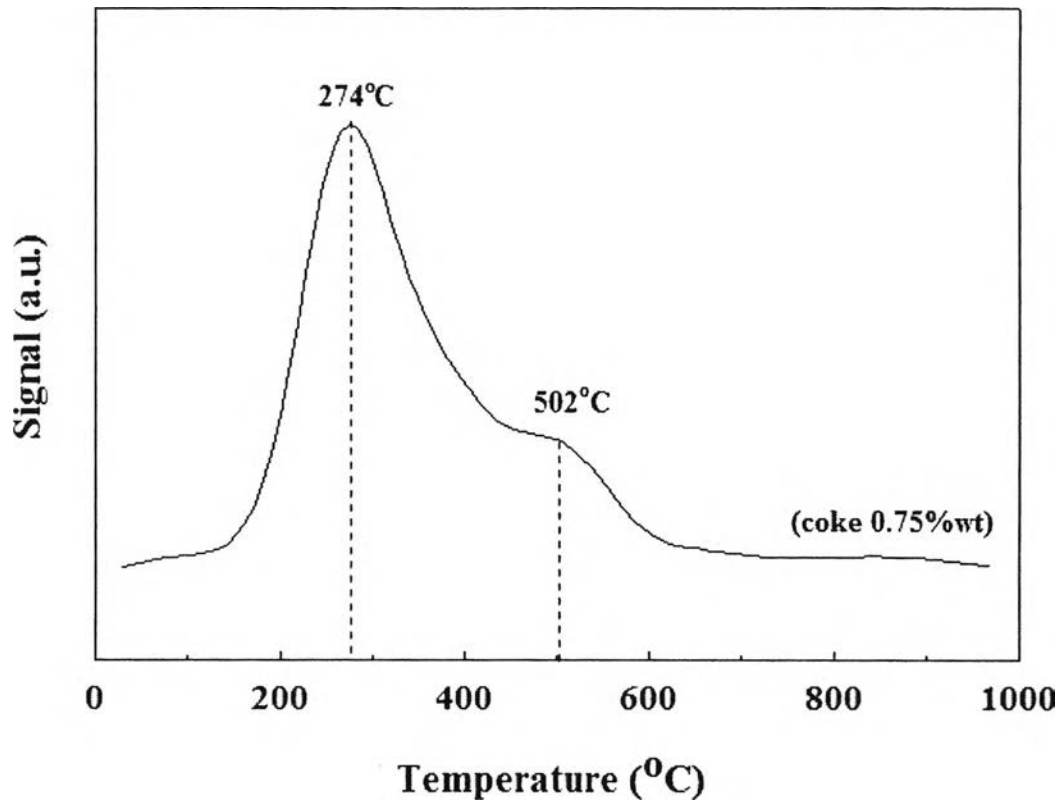

Figure 4.21 TPO profiles of spent 5%wt Au/CeO_2 after exposure to reaction. Reaction conditions: $O_2/H_2O/CH_3OH$ = 1.25/2/1, reaction temperature of 300°C, and time on stream = 168 hours.

4.2.1.2 X-ray Diffraction (XRD)

Figure 4.22 illustrates the comparison of XRD patterns between the fresh 5%wt Au/CeO_2 catalyst and the spent catalyst. Compared to the fresh catalyst, the significant improvement in diffraction of each peak was observed in the spent catalyst after testing the stability test. In addition to Au(111), there was the reflection of Au(200) and Au(220) diffraction could be detectable at 2θ = 44.4° and 64.6°, respectively, in the spent catalyst (Fan *et al.*, 2003). This may be due to the fact that the sintering—only possible reason for this appearance—could take place on the support and gold particle size, resulted in higher particle size. In addition, this effect may also cause the surface alterations such as changes in surface area and pore structure; moreover, this would reduce the dispersion of Au on the surface of CeO_2 and lower its catalytic activity.

As mentioned previously, the sintering of the catalyst during the stability test—causing the larger particle sizes—is the only reason why the spent catalyst has too much higher peak intensities including the appearance of Au(200) and Au(220) compared to the fresh catalyst.

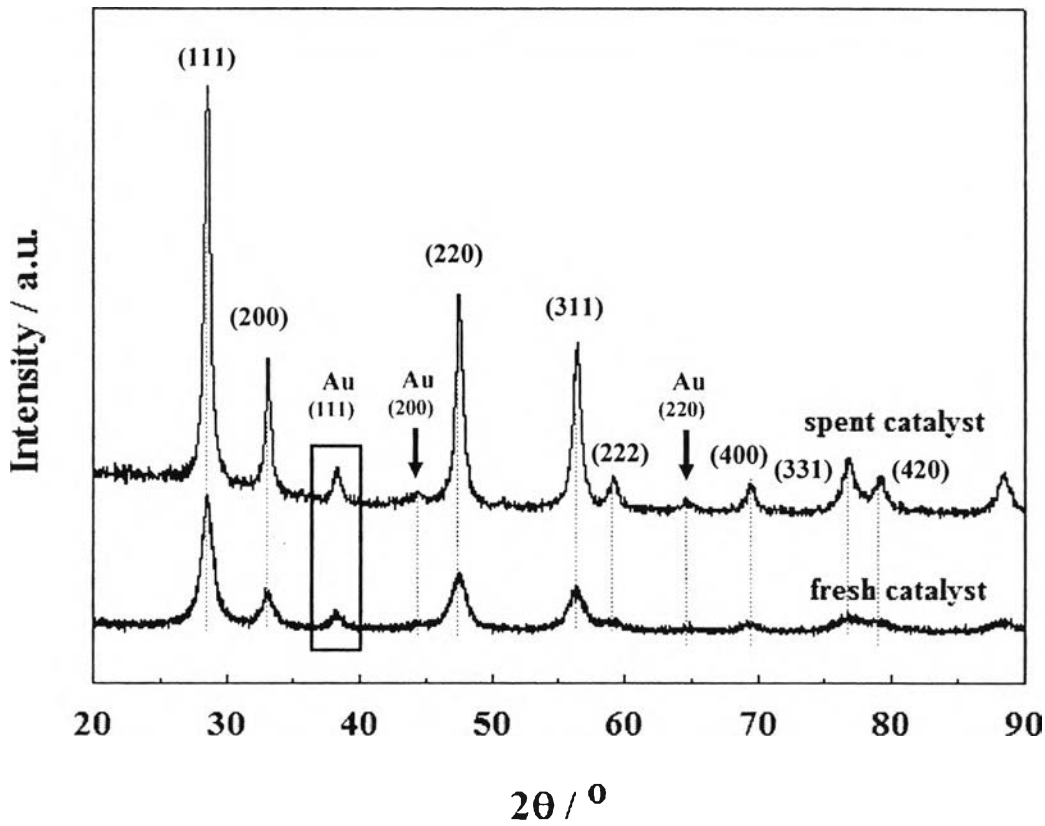

Figure 4.22 XRD patterns of spent 5%wt Au/CeO_2 after exposure to reaction. Reaction conditions: $O_2/H_2O/CH_3OH$ = 1.25/2/1, reaction temperature of 300°C, and time on stream = 168 hours.

4.2.2 Effect of side reactions (DM, POM, and WGS)

By focusing the appearance of three possible mechanism pathways —DM, POM, and WGS—for being the net reaction of OSRM, each of experiment was designed with difference conditions.

To observe the methanol decomposition, which is responsible for the main product from the methanol steam reforming, the experimental values were studied on the basis of the best condition of prepared catalysts—5%wt Au/CeO_2

calcined at 400°C—and reported in Figures 4.23–4.24 within the Eq. 4.5. The reaction conditions were operated at 0.8 ml/hour of liquid flow rate, 50 ml/min of carrier gas (He), and reaction temperature range of 200–400°C.

$$CH_3OH(g) \rightarrow 2H_2(g) + CO(g) \quad \Delta H°_R = 128\ kJmol^{-1}\ (298\ K) \qquad (4.5)$$

Figure 4.23 shows the catalytic activity in the decomposition of methanol reaction. Methanol conversion and hydrogen yield increased as a function of temperature, and the maximum values of 43.45% and 26.21%, respectively, were achieved at 400°C. On the other hand, the lowest values can be obtained at low temperature range (200–300°C) which was responsible for the high activity in OSRM. It can be concluded that the DM reaction didn't play the significant role for improving the methanol conversion and hydrogen yield during the OSRM in the low temperature range. The product distribution of 5%wt Au/CeO_2 in the DM reaction is shown in Figure 4.24. The hydrogen selectivity decreased proportionally with the increase in CO selectivity with reaction temperature. On the other hand, the maximum value of CO selectivity and the lowest value of H_2 selectivity were achieved at 400°C. This could be implied that the DM reaction was the main cause for generating the CO gas during the OSRM reaction. Additionally, the presence of CO gas could lower the H_2 selectivity as well. Nevertheless, there's no methane and carbon dioxide gas observed during the DM reaction.

As mentioned previously about the effect of O_2/CH_3OH molar ratio, the methanol conversion and hydrogen yield were achieved the highest values in the range of low temperature (200–300°C), then the hydrogen yield became lowest after increasing the O_2/CH_3OH molar ratio higher than 1.25/1. This can surely confirm the existence of POM reaction during the OSRM reaction. However, it can be concluded that the POM reaction can help improve the methanol conversion and hydrogen yield significantly during the OSRM reaction in the low temperature range.

For the last mechanism pathway, it is well known in many literature reviews that the Au/CeO_2 catalysts were mostly used to perform the highest catalytic activity in WGS reaction. In this work, the WGS reaction (Eq. 4.6) is one of the side

reactions that existed during the OSRM reaction. Santacesaria and Carra (1983) suggested that the CO formation by DM followed by WGS reaction to produce H_2 and CO_2. In addition, Peppley *et al.* (1999)[1] reported that although DM is much slower than the SRM reaction, it must be included in the overall reaction scheme along with SRM and WGS reactions. Therefore, it is necessary to study the activity of the 5%Au/CeO_2 catalyst in this reaction.

$$CO + H_2O \longleftrightarrow H_2 + CO_2 \qquad \Delta H°_R = -41\ kJmol^{-1} \qquad (4.6)$$

The reaction conditions were 0.3 ml/hours of liquid flow rate at a 2:1 molar ratio of H_2O to CO, a flow of CO of 3.4 ml/min balanced with He, and reaction temperature range of 200–400°C. From Figure 4.25, the CO conversion increased gradually when the temperature increase from 2.93% at 200°C to 7.25% at 350°C. Although the increasing of hydrogen yield as a function of temperature was maximized at the values of 2.06% at 350°C, the very low hydrogen yield could confirm the available WGS during OSRM over 5%Au/CeO_2 catalysts. Nevertheless, the reason why the CO conversion and hydrogen yield were too low in the whole range of reaction temperature was the limitation of the large Au particle size corresponding to the low catalytic activity. In general, many literature reviews proposed that the small gold particle was responsible for the high activity of CO oxidation. Figure 4.26 shows the product distribution of 5%Au/CeO_2 in the WGS reaction. The hydrogen selectivity of 30% was almost constant in all range of temperature studied. As the same trend, the selectivity of CO_2 also kept constant at 70% with the whole temperature range. As a result, it can be concluded that the WGS reaction did not improve the methanol conversion and hydrogen yield too much during the OSRM reaction since the small amount of CO and H_2 product gases.

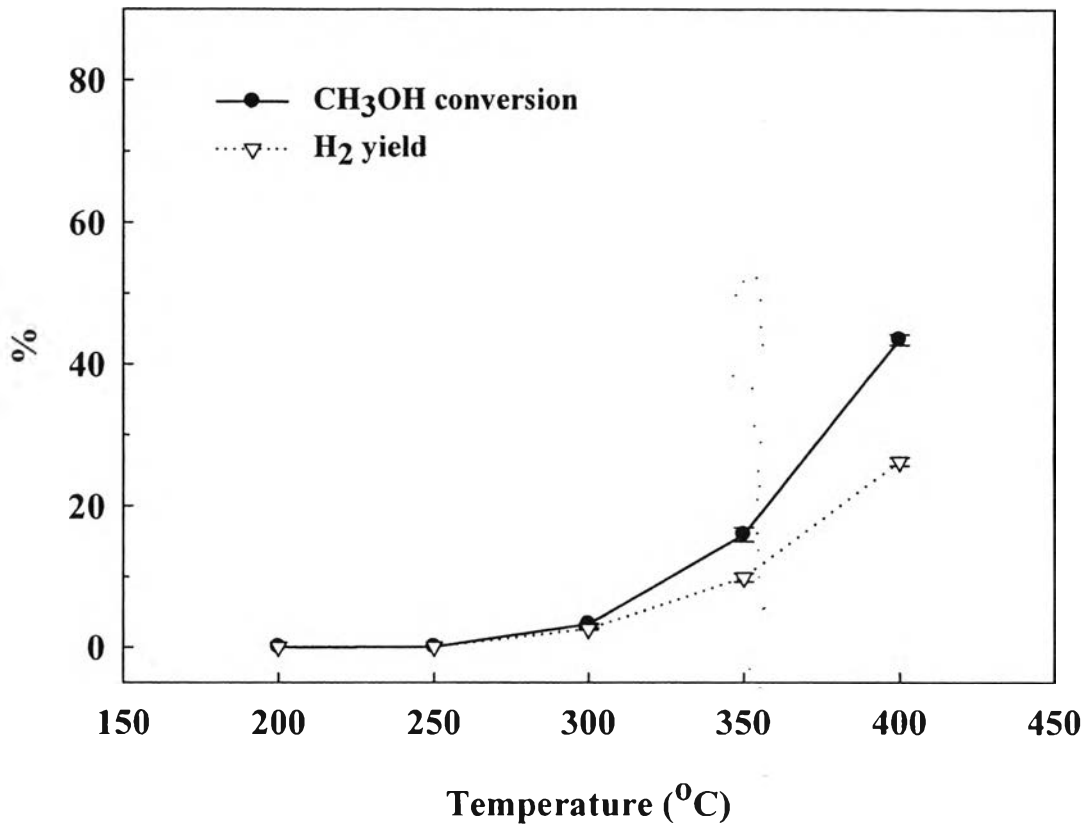

Figure 4.23 Catalytic performance of 5%wt Au/CeO_2 in the decomposition of methanol reaction.

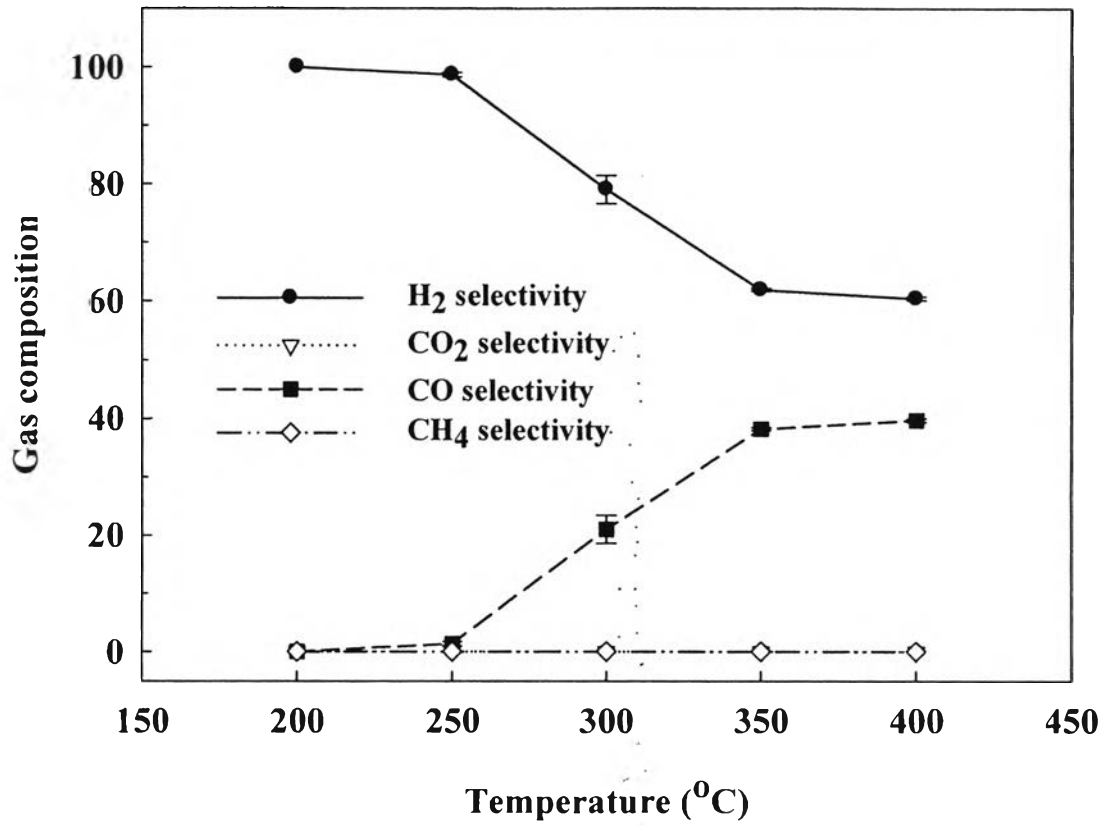

Figure 4.24 Product distribution of the decomposition of methanol reaction.

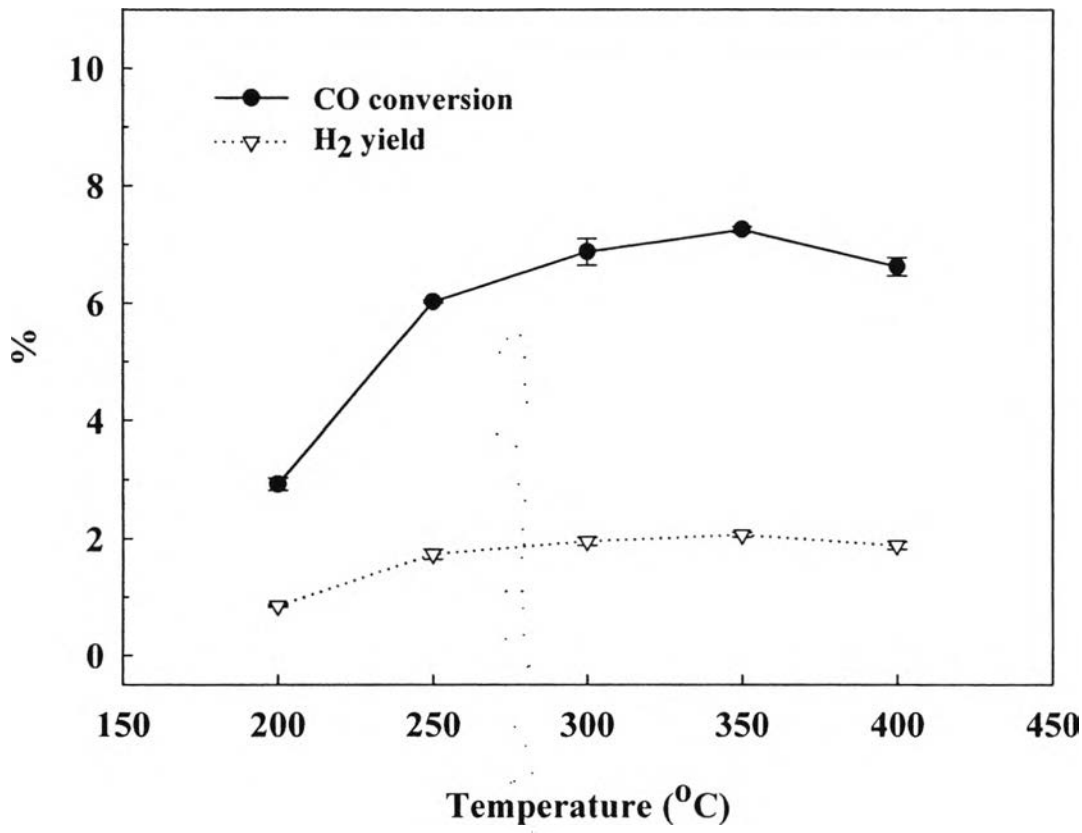

Figure 4.25 Catalytic activity of 5%wt Au/CeO_2 in water gas shift reaction.

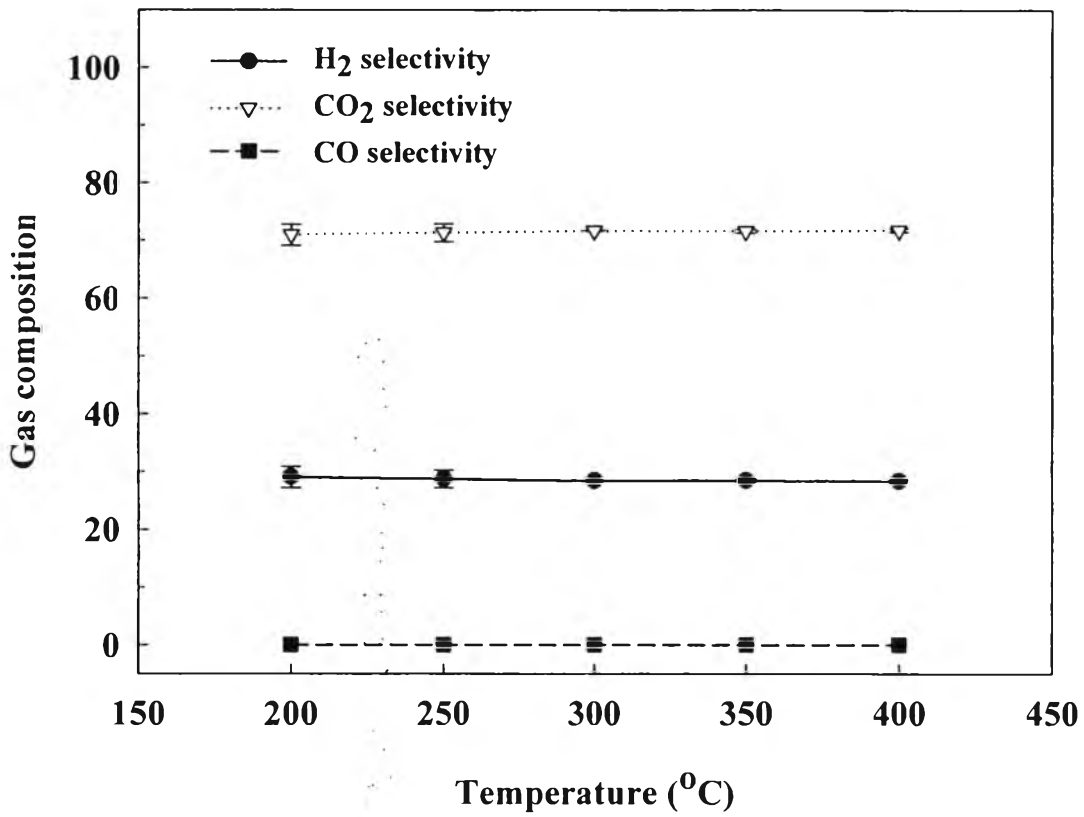

Figure 4.26 Product distribution of the water gas shift reaction.